1-1-2012

A Study of the Microstructural Evolution and Static Recrystallization of Magnesium Alloy AZ-31

Harold Michael Kistler

Recommended Citation

Kistler, Harold Michael, "A Study of the Microstructural Evolution and Static Recrystallization of Magnesium Alloy AZ-31" (2012). *Theses and Dissertations*. 298.
https://scholarsjunction.msstate.edu/td/298

A STUDY OF THE MICROSTURCTURAL EVOLUTION AND STATIC RECRYSTALLIZATION OF MAGNESIUM ALLOY AZ-31

By

Harold Michael Kistler

A Thesis
Submitted to the Faculty of
Mississippi State University
in Partial Fulfillment of the Requirements
for the Degree of Master of Science
in Mechanical Engineering
in the Department of Mechanical Engineering

Mississippi State, Mississippi

May 2012

A STUDY OF THE MICROSTURCTURAL EVOLUTION AND STATIC RECRYSTALLIZATION OF MAGNESIUM ALLOY AZ-31

By

Harold Michael Kistler

Approved:

Mark F. Horstemeyer
CAVS Chair Professor in
Computational Solid Mechanics
Major Professor

Esteban B. Marin
Professor of Mechanical Engineering
Director of Thesis

Bin Li
Assistant Research Professor
Committee Member

Paul Wang
Associate Director CAVS
Committee Member

Steven R. Daniewicz
PACCAR Chair and Head
Graduate Program Coordinator

Sarah A. Rajala
Dean, Bagley College of Engineering

Name: Harold Michael Kistler

Date of Degree: May 11, 2012

Institution: Mississippi State University

Major Field: Mechanical Engineering

Major Professor: Dr. Mark F. Horstemeyer

Title of Study: A STUDY OF THE MICROSTURCTURAL EVOLUTION AND STATIC RECRYSTALLIZATION OF MAGNESIUM ALLOY AZ-31

Pages in Study: 94

Candidate for Degree of Master of Science

The present study focuses on the evolving microstructure of Mg alloy AZ31. The material is subjected to channel die compression at room temperature to simulate a reduction stage in the rolling process. Samples are annealed to provoke recovery, static recrystallization, and grain growth. Annealing is carried out at three temperatures for times ranging from 10s to 10,000s. The material's response is exhibited through the use of data collection methods such as microhardness, optical microscopy, and electron backscatter diffraction (EBSD). Methodology behind experimentation and data collection techniques are documented in detail. Conclusions are made about the effects of the compression and annealing processes on the material's microstructure. The Johnson-Mehl-Avrami-Kolmogorov (JMAK) model is introduced, and a simple recrystallization kinetics plot is attempted.

Key words: AZ31, channel die compression, room temperature, static recrystallization, microstructure, annealing, grain size, microhardness

TABLE OF CONTENTS

APPENDIX

LIST OF TABLES

LIST OF FIGURES

CHAPTER I

INTRODUCTION

This section describes the general motivation of the present research, a brief explanation of the objectives to be completed in this study, and a short overview of the steps included in researching this material. At the end, some remarks are given about the effort to be undertaken to complete this research.

1.1 Purpose For Study

The ability to modify a material's mechanical properties is important for many industrial applications. Changes made to a material's microstructure can allow for modifications in properties such as formability, strength, and toughness. Having the capability to manipulate a material in this sense allows for its use in applications that have previously seemed impractical. For this reason, the ability to understand the mechanics of the microstructure evolution of a material when it is subjected to load, temperature, and environmental changes is of high interest in industry.

Due to its low formability, and lack of slip bands at room temperature, Mg alloys are usually formed at high temperatures, an aspect overlooked for many applications in the past. However, the light weight and strong structural properties of Mg make it appealing for both the automotive and aerospace industries. Recently this has lead to a renewed interest in Mg alloys, in particular Mg AZ31, for structural applications. Although there has been an increase in the research of Mg alloy AZ31, only few studies have examined the static recrystallization and grain growth of this material. Studying these phenomena requires a careful experimental plan to produce microstructures in a large amount of samples subjected to various thermo-mechanical histories. This proves to be a very long and tedious task. Hence, because of the lack of information regarding this topic, it is of considerable significance to observe the kinetics of statically recrystallized AZ31 subsequent to cold deformation and annealing.

1.2 Objective of Thesis

The main purpose of this study is to characterize the microstructural evolution of magnesium alloy AZ31 under specified deformation and heat treatment conditions. In particular, the work will focus on studying static recrystallization phenomena through annealing experiments on specimens deformed under plane strain compression. For this purpose, the following tasks have been identified:

1. Experimentally create a compression method that simulates a room temperature reduction stage in the rolling process.
2. Capture the materials response to the specified deformation and heat treatment techniques, and obtain data that describes the evolution of the material.
3. Calculate and graph the static recrystallization process, determined by both hardness data and electron backscattering diffraction.
4. Use the collected data to determine the trend for static recrystallization and describe the material's microstructural evolution.

1.3 Research Overview

In order to obtain the data needed to accomplish the objectives of this study, a set of experimental testing, heat treating, and data analysis methods were formulated, and a brief description of these tasks are listed below. These procedures are later described in detail in chapters III, IV, and V.

1. Compress samples at room temperature and heat treat them at several temperatures for times ranging from 10s to 10,000s.
1. Collect Vickers hardness data from microhardness indentation to display the materials hardness evolution and represent the rate of recrystallization for several temperatures.
2. Perform Optical Microscopy on the samples to visually display the grain evolution of the material's microstructure.
3. Run Electron Backscattering Diffraction scans on chosen samples to collect data showing the progression of grain size evolution, material orientation, and calculating sample Recrystallization fractions determined from electron backscattering diffraction statistics.

1.4 General Remarks about this Work

Capturing the evolution of a materials microstructure can prove to be a very tedious and time consuming task. Because the materials being studied have typically undergone some kind of transformation, developing a consistent methodology for testing and observing the samples evolution can involve a great deal of revision on a sample to sample basis by the experimentalist and those who are collecting data and analyzing the results. To fully capture the materials response and be able to confidently predict and model its evolution, a series of tests and data analysis need to be performed. Because AZ31 has demonstrated its sensitivity to temperature, strain rate, deformation, and anisotropy, the material should be observed subsequent to deformation at several strain rates, strains, and temperatures that allow for the capturing of both the static and dynamic recrystallization processes that can occur during the evolution of the microstructure.

CHAPTER II

LITERATURE REVIEW

This chapter presents a review of literature relevant to the present study. Several frequently used metal forming processes are described along with their effects on material properties. The fundamentals of both static and dynamic recrystallization are discussed, together with some aspects of nucleation, grain growth, texture, and grain orientation. Numerous papers, specifically dealing with experimental studies on AZ31, are also explored to help gain an understanding of the material's response to various conditions. The later part of this chapter discusses the concepts of modeling and simulation as well as several cases involving the modeling and simulation of AZ31.

2.1 Metal Forming Processes

There are many forming processes applied daily for a variety of industrial applications. Metal forming is defined as a fabrication process of solid materials by controlled plastic deformation in order to attain modifications of form, material properties, and surface properties. Through this process the mass and the material continuum remain unchanged (Banabic 2000). In general, both billet and sheet metal forming are included in metal forming. It is well accepted, however, to divide these processes into two groups. The first group is bulk forming. This group includes forging, rolling, drawing, and extrusion. The second group is sheet metal forming. This method includes the production of a wide variety of shapes within thin walls and either complex or simple geometries. In particular, the present work will study the effect of the rolling process on material deformation and microstructure through channel die compression experiments which mimics the stress state (plane strain compression) at the center of a workpiece in a rolling process. Before focusing on the specific forming process of interest, some general characteristics of metal forming will be described such as flow stress and plastic flow under combined stresses.

2.1.1 Characteristics of Metal Forming

Flow stress, also known as true stress, is basically a material's resistance to plastic deformation. Therefore, it can be determined that under a uniaxial state of stress, the flow stress of a material is the stress required to initiate or continue plastic deformation (Hamrock et al. 1999).

$$\text{Flow Stress:} \quad K_f = \frac{F}{A} \qquad \text{Technical Stress:} \quad \sigma = \frac{F}{A_0} \tag{2.1}$$

The flow (true) stress takes into account the change in area (A), while the technical (engineering) stress is simply the applied force divided by the original cross sectional area A_0. When a material is under a multiaxial stress state, there are certain requirements that must be fulfilled for plastic deformation to occur. If the applied stress, represented by the equivalent stress (σ_v), is equal to the flow stress (K_f), then the criteria for plastic flow is met. Typically, the equivalent stress is derived using either the shear stress hypothesis or the forming energy hypothesis (Kobayashi et al. 1989). Based on the distortion energy (Von-Mises) theory, flow sets in when the elastic distortion energy for changing the form exceeds a critical value,

$$\sigma_v = k_f = \sqrt{\frac{3}{2}\left((\sigma_1 - \sigma_m)^2 + (\sigma_2 - \sigma_m)^2 + (\sigma_3 - \sigma_m)^2\right)}$$

$$where \quad \sigma_m = \frac{1}{3}(\sigma_1 + \sigma_2 + \sigma_3) \tag{2.2}$$

where $\sigma_1 > \sigma_2 > \sigma_3$ are the principal stresses and σ_m is the average (mean) stress (Hamrock et al. 1999).

2.1.2 The Rolling Process

The roll forming process is a type of metal forming that can be performed at either room or elevated temperatures. This process is known as cold rolling when it is performed at room temperatures or hot rolling when performed at higher temperatures. This process has widely spread throughout the world and can often be found in numerous applications. One of the main reasons for the popularity of this process can be contributed to its ability to be used in collaboration with auxiliary operations such as punching and welding. This feature allows for the production of profiles which are directly ready for use (Brunet et al. 1998).

Rolling accounts for approximately 90% of all metals produced by metalworking processes, and can be described as the process of changing the cross sectional area or thickness of a workpiece by applying compressive forces through a set of rollers. The basic rolling process is used to produce flat plates or sheets (strips). Plates and sheets are generally regarded as having thicknesses greater than 6mm and less than 6mm, respectively.

Typically, rolling is performed at elevated temperatures, promoting dynamic recrystallization and causing the coarse-grained brittle structure to transform into a wrought structure with improved properties and a refined microstructure. This transformation results in good ductility and improved strength (Farag 1990).

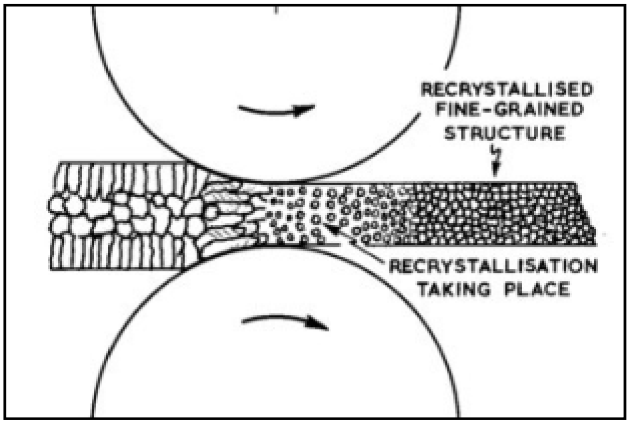

Figure 2.1 Recrystallization during the hot rolling process.

However, the rolling process can also be performed at room temperature.

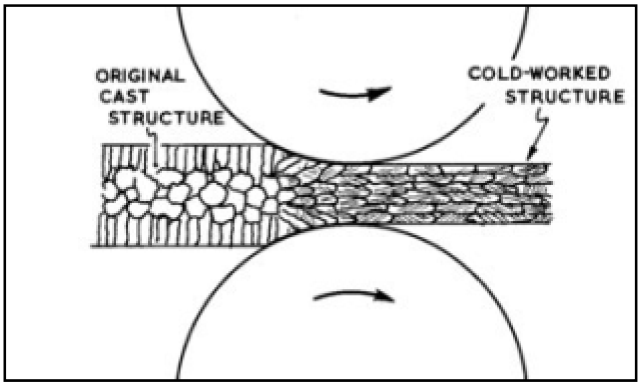

Figure 2.2 Work hardening of a cold rolled metal.

This process results in work hardening of the material. Unlike hot working, where deformation occurs simultaneously with recovery and recrystallization, cold working is deformation under conditions where these recovery processes are not effective. Several structural changes occur during the cold working of a material (Honeycombe et al. 1968):

1. Grains are elongated in the direction of the acting force and they are stretched in the rolling direction.

2. The preferred orientation or texture of the grains is with respect to the direction of the stress.
3. Around 15% of deformation work is absorbed in the internal structure of the grains and the rest is lost due to heat. Stored energy is in the form of crystal defects. The plastic deformation causes an increase in the concentration of point defects and there is an increase in dislocation density.

Along with changing grain structure, cold working can cause changes in various mechanical properties as well. Increasing the amount of cold work will result in a higher ultimate tensile strength, yield strength, and hardness, as well as a decrease in ductility of the material. Because cold worked materials do not undergo the recrystallization process during deformation, these materials are often annealed to evolve the material's microstructure to obtain the desired characteristics. The annealing process can be separated into three stages: Recovery, Recrystallization, and Grain growth (F. J. Humphreys & Hatherly 2004). Recovery and Recrystallization are driven by stored energy due to deformation, while energy stored in grain boundaries are the driving force for grain growth:

1. Recovery, although causing no observable changes in the microstructure, restores the physical properties to the material. It can be noted that during this stage point imperfections and dislocations are rearranged and discarded without the migration of high angle boundaries. Initially recovery is very fast and it increases with higher annealing temperatures and larger deformation. However, it becomes slower over time. Recovery is also grain size sensitive, allowing for a higher rate of recovery for finer grains.

2. Recrystallization is the nucleation and growth of new strain-free crystals. There are two distinct nucleation mechanisms that have been identified for the kinetics of recrystallization. The first is Strain-induced boundary migration. This occurs when a strain free recrystallized region is formed by a coalescence of pre-existing grain boundaries into each other. Second is the formation of new grains in regions of sharp lattice curvature through subgrain growth. This mechanism seems to occur more frequently at high strains and can be seen by nuclei forming around grain boundaries or inclusions. Because there are so many factors that affect recrystallization, such as deformation, temperature, time, and grain size, the recrystallization temperature is not fixed with respect to a materials melting point. Instead, it is defined as the temperature at which the given alloy completely recrystallizes in one hour.
3. Grain Growth is the stage following recrystallization and results in a uniform increase in average grain size. Grain growth can either be normal or abnormal. During normal grain growth, the grain size distribution does not change. However, during abnormal grain growth, the presence of both large and fine grains may be observed. This abnormal growth is caused by a decrease in surface energy.

Figure 2.3 provides a visual representation of how a material's mechanical properties typically change with respect to the recovery, recrystallization, and grain growth processes.

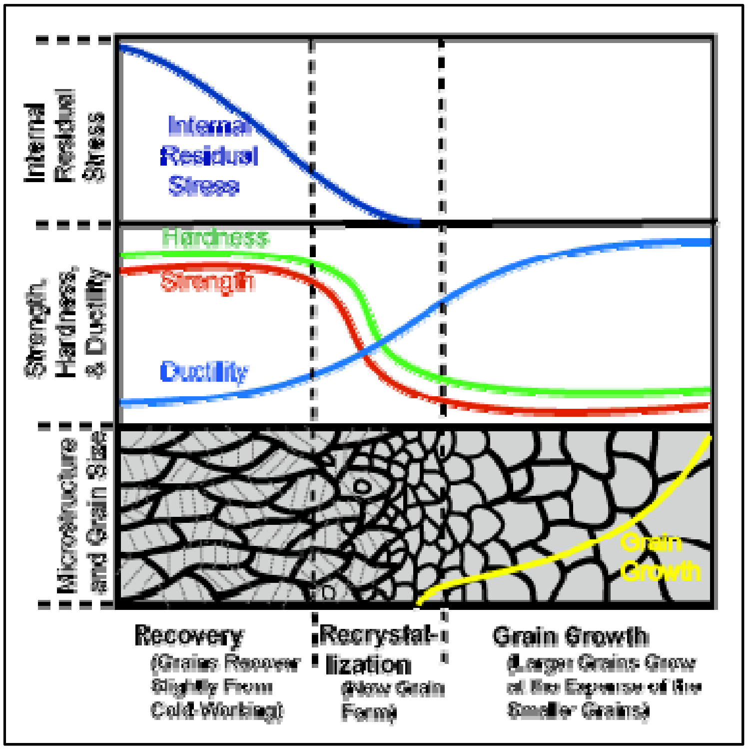

Figure 2.3 The comparison of mechanical properties during recovery, recrystallization, and grain growth.

2.2 Plane Strain Compression

Strain deformation testing has become a very important requirement for the formulation of constitutive equations used in finite element simulations for many shaping operations such as rolling and forging. Channel die compression is an excellent replacement for industrial rolling processes for experimental purposes because it limits spreading of the material in the lateral direction while allowing deformation along the length of the channel. However, channel die testing has not been highly utilized at room temperature because of its reputation for friction problems. Despite issues with friction, the channel die method has been used successfully in several applications since it has been shown that proper lubrication techniques can overcome difficulties involving friction. This procedure is validated through the comparison of data obtained from metallographic analysis, flow stress, and microstructure measurements obtained by hot channel die experimentation and alloys deformed using conventional compression methods (Maurice et al. 2005). The effects of plane strain compression were also investigated by (Raabe et al. 2001), both experimentally and through simulation (continuum FE and crystal plasticity FE with non-zero friction). It has been determined from this study that strain localization occurs along the diagonals, with the maximum occurring at the corners, and the localized strain lessens towards the center of the sample. The strain profile created from plane strain compression with non-zero friction is found to be principally similar to the strain profile obtained from crystal plasticity simulation and experimentation. The complexity of a sheets rolling production schedule determines its cost and mechanical properties, and the amount of complexity usually involves edge stress accumulation. This can result in defects, cracking, and substandard mechanical properties. However, rolling can result in a strong crystallographic structure. Rolled Mg alloys display asymmetric strength properties in the tension and compression directions. The {1012} twinning mechanism parallel to the HCP c-axis accommodates tensile strain and not compressive strain. Therefore, a stronger basal texture will provide a stronger asymmetry between the tension and compression directions (Sediako et al. 2007). A study performed by (Nave & M. R. Barnett 2004) compressed pure Mg samples in a channel die at room temperature. One objective of the study was to examine the differences in samples compressed along the c-axis and perpendicular to it. The anisotropic behavior is evident when comparing the true stress and true strain curves of the two types of specimens. The results from this study are located in Figure 2.4.

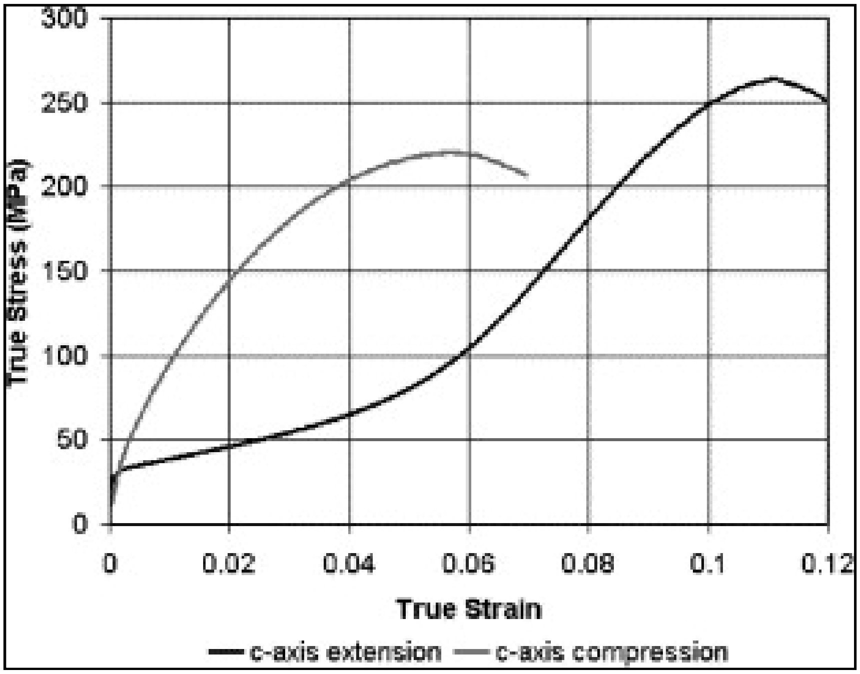

Figure 2.4 True-stress versus true-strain curves for samples subjected to plane-strain compression with *c*-axis extension and *c*-axis compression. Each curve represents the average of two tests and has been truncated shortly after the peak stress, close to the point of failure.

The material's tress strain path can be attributed to the material's initial textures and how the loads are applied to the samples. The associated slip and twinning planes contribute greatly to the material's change in texture. (Choi et al. 2011) describes four of the common slip systems found in the AZ31 alloy which are shown in Figure 2.5. It is explained that the roles of these slip systems, as well as the twinning system, are highly associated with how the material deforms.

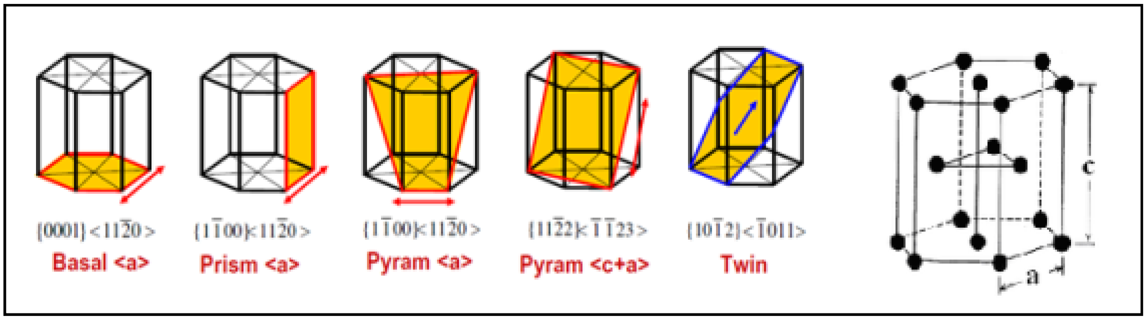

Figure 2.5 Four of the common slip systems and one twin system found in AZ31; Basal <a>, prismatic <a>, pyramidal <a>, pyramidal <c + a> slip systems and tensile twin system for HCP materials.

The texture observations by (Nave & M. R. Barnett 2004), both before and after channel die compression are available in Figure 2.6. They reveal that after undergoing deformation the c-axis for both samples align with the compression direction.

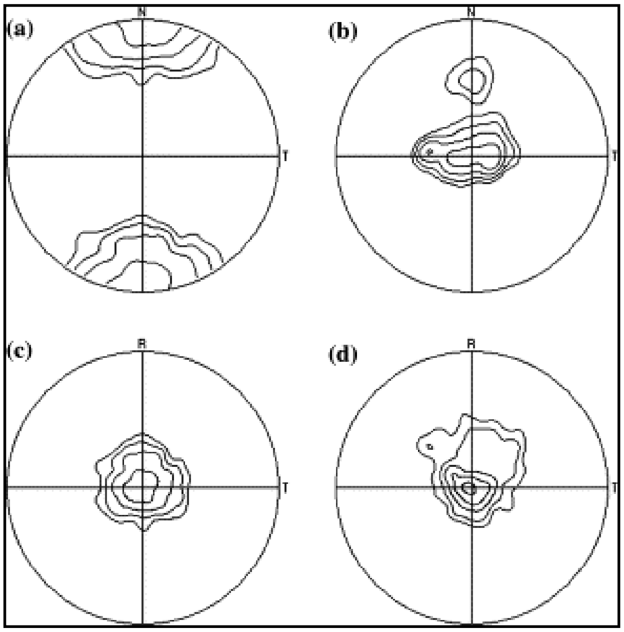

Figure 2.6 {0 0 0 1} pole figures showing initial (a,c) and pre-failure (b,d) textures for the *c*-axis extension (a,b) and *c*-axis compression (c,d) channel die samples. The compression direction is at the centre of each pole figure, while the extension direction is directed up the page. The labels show the rolling (R), transverse (T) and normal (N) directions of the hot-rolled sheet from which the samples were cut. Contours represent intensities of 1, 2, 4, 8 and 16× random.

It can be determined that the anisotropic mechanical behavior of HCP materials is strongly influenced by the crystallographic texture evolving during the forming process. The asymmetry can significantly be seen in rolled sheets of AZ31 when observing the flow stress in compression and tension. The strong basal texture of the material is responsible for the dissimilarity, allowing twinning in compression but not in tension.

2.3 Recrystallization

There are two main reasons that the recrystallization of plastically deformed metals and alloys is important to the processing of metallic alloys. The first can be explained by the idea that when a material is deformed at low temperatures, the material is hardened. Recrystallization will restore ductility and soften the material. The second reason is the idea of controlling the grain structure of the final product (F. J. Humphreys & Hatherly 2004). During the deformation of a material, energy becomes stored mostly in the form of dislocations. The stored energy is then usually released through recovery, recrystallization, or grain coarsening. Grain coarsening will either occur by normal grain growth (the disappearance of the smallest grains) or the abnormal grain growth (the enlargement of a few grains much larger than the average grain size of the material). Grain coarsening is driven by the reduction of the grain boundary area which results in the growth of the mean grain size. Recovery, involves the lowering of energy through the rearrangement of dislocations which can be seen through the formation of low-angle sub-grain boundaries (Martin et al. 1997). For this study, the method of energy release of most interest is that of recrystallization. Recrystallization can be defined as the formation of a new grain structure by the migration and formation of grains with a misorientation greater than 10 – 15°. These newly formed grains are known as high angle grain boundaries that are a result of stored energy from deformation (F. J. Humphreys & Hatherly 2004). Recrystallization can be broken down into two main processes: nucleation and grain growth, both of which will be discussed in this section.

2.3.1 Nucleation and Grain Growth

There are two types of structural transformations. The first one is Gibbs I, or better known as "nucleation and growth". In this transformation, the structural change is limited locally with a defined boundary between the old and new structure, but is extensive with respect to the overall magnitude of change. The second transformation is Gibbs II or "homogeneous". This change occurs throughout the entire material. However, the change in structure is initially small. Normal grain growth is considered a Gibbs II transformation, while abnormal grain growth and recrystallization are classified as Gibbs I transformations. A Gibbs I transformation can be broken down into two steps: The initial formation of a new grain and the growing of the new grain (F. J. Humphreys & Hatherly 2004).

Cahn proposed in 1949 that new grains do not nucleate as completely new grains, but that these new grains grow from small recovered subgrains that already exist in the deformed microstructure (Cahn 1950). This theory has been confirmed experimentally many times (Haessner 1978). As a result, the orientation of each new grain comes from the orientation of the deformed state. Haasen showed that the development of new orientations can be caused by growth twinning of growing new grains that occur in low energy materials (Haasen 1993). A very similar situation occurs in abnormal grain growth. A small portion of the existing grains start to grow at the expense of the majority of the other grains, which do not seem to mature with any significance. Like the new grains in recrystallization, the new grains in abnormal grain growth evolve from pre-existing embryos present in the deformed structure. Based upon recrystallization studies of aluminum (R. Doherty, Hughes, et al. 1997), it is evident that only a small proportion of Cahn's subgrains make the transition to a recrystallization nucleus. The theory that nucleation only takes place in the microstructure at regions with high local misorientation is widely supported by (Cottrell 1953) and many others. His reasoning for the low probability of transformation was attributed to the low mobility of the subgrain boundaries. He stated that the majority of subgrains have only a small misorientation with their neighbors, and that only subgrains with a high misorientation angle to the deformed material would have enough mobility to evolve into the recrystallized grains.

As stated earlier, nucleation sites require a large amount of local misorientation. Therefore, according to Doherty (R. Doherty, Hughes, et al. 1997), some typical nucleation sites include:

1. Places where high angle grain boundaries previously existed
2. Misoriented "transition" bands inside grains, between parts of the grain that have undergone different lattice rotations. The difference in rotation is due to the activation of different slip systems
3. Deformation zones around large particles that are highly misoriented
4. In highly misoriented regions of shear bands
5. Locations that have been very heavily deformed within the material

An interesting topic has been studied relating to the strong recrystallization texture that often occurs after large deformation. It has been noticed that after only a small deformation, the textures produced are almost random. Annealing of highly deformed samples has proven to result in a very different, but very strong, new recrystallization texture. To help in the understanding of how different grain sizes might occur, Juul Jensen (Hansen, D. Jensen, et al. 1995) hypothesized that a recrystallizing grain growing in a very highly deformed material will meet many other areas of different orientation. On the other hand, grains with orientations within the deformation texture will meet similar orientations causing a lower mobility and slower growth.

2.3.2 Development of Misorientation

The development of textures and microstructures during deformation determine the changes that occur in the material during recrystallization. The division of grains into differently oriented regions characterizes deformation microstructures. These rotated regions are separated into small and large strains by dislocation boundaries. Since deformation structures are so complex, they have been classified based on their misorientation, morphology, spacing, and orientation (Bay et al. 1992).

Diverse crystal orientations throughout a grain can be attributed to the development of misoriented dislocation boundaries. The range of orientation within a grain varies from small differences to very large differences. An increase in strain causes an increase in the range of different orientations, and the large differences can be related to the complex spatial patterns of orientations (Hansen, D. Jensen, et al. 1995). Depending on the grain orientation, grain subdivision can lead to an uneven distribution of stored energy as well as a large distribution of misorientated angles across dislocation boundaries.

If an annealed material is considered, there may be a formation of nuclei among the deformed microstructure. If a nucleus is surrounded by a high angle boundary it may be able to migrate into the deformed microstructure resulting in growth of the nucleus.

This high angle boundary may be related to the high angle boundary that was present in the deformed structure, or it may be a result of the annealing process. High angle boundaries that are formed during the annealing process are known as annealing induced while those boundaries formed during deformation of the material are classified as deformation induced (F. Humphreys 1999). Stored within the deformed material matrix, lies the energy that provides the driving force for the migration of annealing induced boundaries. The mobility term M, and the driving force Δf make up the velocity of the migration of the annealing induced boundaries.

$$V = M \bullet \Delta f \tag{2.3}$$

2.3.3 Texture Evolution

During recrystallization, the texture may evolve so dramatically that it is almost completely replaced by an entirely new texture. A strong deformation texture will be replaced with another strong recrystallization texture based upon the nucleation and growth process. Once a material is plastically deformed there is work stored inside the structure. However, this stored energy is eliminated with the growth of new grains that may have a different orientation (R. Doherty, Hughes, et al. 1997). However, when there is a large volume fraction of second phase particles or when a material has undergone axisymmetric deformation, recrystallization does not always result in large changes in texture. By summing over the texture components in a recrystallized system, it is possible to relate texture evolution to the boundary properties of specific components. Assuming that an average of all the components present in an unrecrystallized region allows for use of the JMAK model where F_i is the volume fraction recrystallization of the ith term, and dF^x is the extended volume fraction increment.

$$dF_i = (1 - F_{total}) \, dF_i^X \tag{2.4}$$

$$dF = \sum_I dF_i \tag{2.5}$$

(R. Doherty, Hughes, et al. 1997) suggests that there is a great need for the computer simulation of recrystallization for two main reasons. The first is the need to be able to predict the microstructure and material properties after the annealing process. The second is the need to improve the understanding of what happens to the texture and microstructure during the recrystallization process. If the process depends on the misorientation between regions and the shapes of these regions, a model with the capabilities of simulating both the idealized and realistic microstructure must be used.

2.3.4 Grain Boundaries

Grain boundaries play a role in recrystallization as well. The boundary where two single-crystal grains meet in a polycrystalline material is known as a grain boundary (Merkle & Wolf 1990). It is well accepted that recrystallization is advanced by the migration of new grain boundaries into the deformed matrix. This cannibalistic like behavior leaves behind what are known as strain free grains. The migration is caused by the presence of the deformed structure on one side and recrystallized structure on the other, which form an energy gradient across the boundary (Gleiter & Chalmers 1972). Typically grain boundaries are described by the misorientation of one grain with respect to another (Grimmer 1974). Many times, grain boundaries are grouped into classes, such as low and high angle, twist and tilt, and special and random. The first class is defined by structure and energy criteria whereas the latter two classes are strictly geometrical. At an angle of 15° it becomes nearly impossible to separate dislocations forming the boundary. Therefore, this angle has become the accepted angle separating low and high angle boundaries. It has been established that the mobility of a grain boundary, M, is:

$$M = \frac{v}{P} \tag{2.6}$$

where v is the velocity of the advancing grain boundary, and P is the driving force (Molodov et al. 1995). Since low angle boundaries migrate slower than high angle boundaries, it is expected that high angle boundaries dominate the recrystallization process.

2.4 Previous Studies of AZ31

Because magnesium is a hexagonal close-packed metal, its deformability is limited at low temperatures due to a lack of operative slip systems. As a result, there is a need for more studies that look into the recrystallization of magnesium, especially at low temperatures. However, because of its strength, stiffness, machinability, and recycling capability, it is very attractive for automotive and aerospace applications. Since Mg possesses such desirable qualities, many studies have been performed on this metal as well as its alloys. One of the alloys in particular interest is AZ31. Previous literature has shown the effects of temperature, strain and strain rate, and twinning on the alloy. A summary of these studies is presented in this section.

2.4.1 Temperature Effects

Most plastic deformation processes dealing with Mg take place at temperatures above 50% of the absolute melting temperature. Deformation at these high temperatures almost ensures recovery and recrystallization, both of which assist in the increase of formability. Annealing processes are frequently used in deforming Mg because of their significance during material processing for two main reasons. They help soften the material and restore formability and ductility. Also, the recrystallization of a material produces a new grain structure with modified properties. Control over the grain structure can be very beneficial. According to C.W. SU (Su et al. 2008), for isothermal annealing between temperatures 200°C – 400°C the kinetics of grain growth could be described by:

$$D^n - D^n_0 = c_1 t \quad \text{where n varies from 2.4 to 3.8} \qquad (2.7)$$

It was discovered that the grain growth exponent (n) is temperature dependent and that the increase in n from pure magnesium was caused by the alloying atoms. Another similar study was performed by A.G. Beer (Beer & M. Barnett 2008a). It was concluded that the behavior of annealed AZ31 is consistent with what is expected for a recrystallization reaction. The rate of grain coarsening was also found to be rapid at the highest temperature and strain rate. Commonly, the microstructure develops faster with increasing temperature. It has been noted that not much change in microstructure is observed at temperatures up to 100°C. However, the most significant changes in microstructure occur within a few minutes at temperatures above 300°C (Jäger et al. 2006). The static recrystallization kinetics of cold drawn AZ31 were studied by (Chao et al. 2011). The samples were cold drawn at room temperature and then subjected to various annealing treatments. They found that annealing temperature had more of an effect on average grain size than holding time. The moderate annealing temperatures resulted in grain refinement, while temperatures above 350°C led to abnormal grain growth. The JMAK model was able to describe the static recrystallization kinetics for temperatures between 210°C – 300°C. The samples annealed at 300°C resulted in a fully recrystallized material in less than 100 seconds. Based on the majority of experimentation performed on temperature effects on AZ31, it can be concluded that an increase in temperature produces more favorable recrystallization textures and mechanical properties (Guo et al. 2005). The influence of annealing the AZ31 material is also investigated by (Jäger et al. 2006). The samples were subjected to tensile tests at room temperature and then annealing at temperatures ranging up to 400°C. It is noted that not much change is seen between the annealing of the material at 300°C and 200°C. However, there is a significant increase in the rate of recrystallization at the higher temperature. The most significant changes occur in just a few minutes. Two minutes of annealing at 300°C is enough to fully recrystallize the material and remove almost all of the twins. This trend is also seen in the higher temperatures as well. At 400°C, 60 seconds of annealing results in a significant change to the microstructure. It is concluded that higher temperatures cause the onset of microstructural changes and recrystallization to occur earlier, and longer annealing times proved to result in a more homogeneous microstructure with larger grains.

2.4.2 The influence of Strain and Strain Rate

Strain rate has an influence on material as well as temperature. (Beer & M. Barnett 2008a) studied the effects of annealed AZ31 after hot compression. The samples were compressed at temperatures ranging between 300°C – 400°C at several strain rates. It was observed that larger grains are developed with increasing annealing times, with the degree of grain coarsening being larger for the samples deformed at lower strain rates. For the samples annealed at the highest strain rate, the microstructure remains unchanged after 100 seconds. Samples deformed at the lowest strain rate (.001-s) display a still evolving microstructure even at 10,000 seconds. Therefore, it is concluded that a stable annealed grain size is obtained earlier for higher deformation rates. The annealing effects on AZ31 studied by C. W. SU (Su et al. 2008) demonstrated that the recrystallization temperature of cold-deformed AZ31 was a function of deformation strain. At strains below 0.1 recrystallization only occurred at temperatures above 300°C. However, when the strain was increased above 0.3, recrystallization was seen at temperatures around 150°C. Another investigation into the effects of strain and strain rate on the dynamic recrystallization process for AZ31 was carried out by (Fatemi-Varzaneh et al. 2007). The purpose of the study was to observe the effects of temperature and strain rate on the microstructural evolution of the material. Their results convey that at higher strain rates, more stress is required to deform the material. As expected, higher temperatures allow for deformation at lower stress levels. The microstructural observations indicate that for a constant strain, as the strain rate is increased, the volume fraction of the grains is reduced. However, an increase in temperature under these conditions results in an increase in recrystallized percentage. It was also observed that at a constant temperature, an increase in strain resulted in more recrystallized material as well. These conditions resulted in increased grain size as well up to around 0.2 strain. After this level of strain, little increase in grain size was observed.

2.5 Modeling and Simulation

As the interest in magnesium alloys increases, new methods for tracking the transformation of the material arise. Because the recrystallization process plays such a major role in the development of a new material and its properties, many investigations have been carried out trying to model and simulate both the static and dynamic recrystallization process in AZ31. In this section, some of these studies and their methods will be described.

By means of relaxation method experiments, (LEGERSKI et al. n.d.) were able to successfully implement experimentation into their model describing the static recrystallization of AZ31. It was found that at temperatures above 250°C, the material is able to fully recrystallize. This model should prove useful in forming processes carried out at lower temperatures. The data collected from the experiments was tabulated and applied to equations describing the recrystallization process of the material. A comparison of the experimental recrystallization values and the model prediction are provided in Figures 2.7 and 2.8.

$$X = 1 - \exp\left(-\ln(2)\left[\frac{t}{t_{0.5}} \right]^{0.7} \right)$$

$$t_{0.5} = 6.8 \cdot 10^{-4} \varepsilon^{-0.35} \gamma^{-0.04} d_0^{0.24} \exp\left(\frac{29950}{RT} \right) \tag{2.8}$$

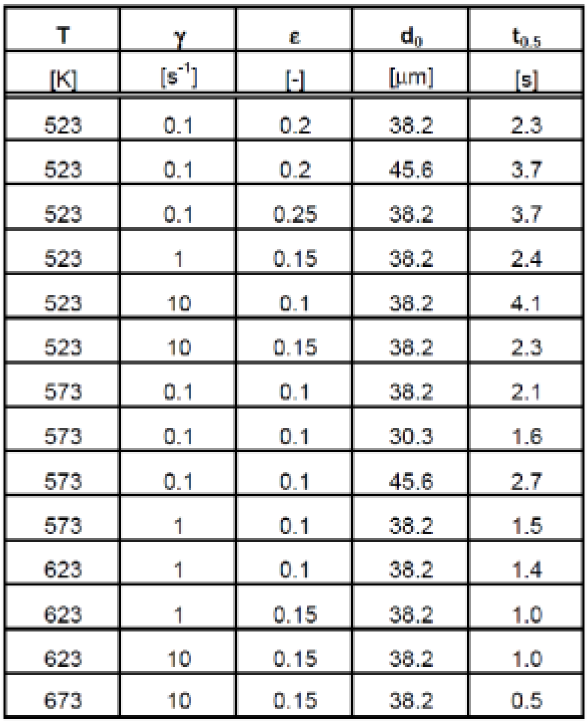

T	γ	ε	d_0	$t_{0.5}$
[K]	[s^{-1}]	[-]	[μm]	[s]
523	0.1	0.2	38.2	2.3
523	0.1	0.2	45.6	3.7
523	0.1	0.25	38.2	3.7
523	1	0.15	38.2	2.4
523	10	0.1	38.2	4.1
523	10	0.15	38.2	2.3
573	0.1	0.1	38.2	2.1
573	0.1	0.1	30.3	1.6
573	0.1	0.1	45.6	2.7
573	1	0.1	38.2	1.5
623	1	0.1	38.2	1.4
623	1	0.15	38.2	1.0
623	10	0.15	38.2	1.0
673	10	0.15	38.2	0.5

Figure 2.7 The tabulated experimental data for varying strains and strain rates, for three temperatures.

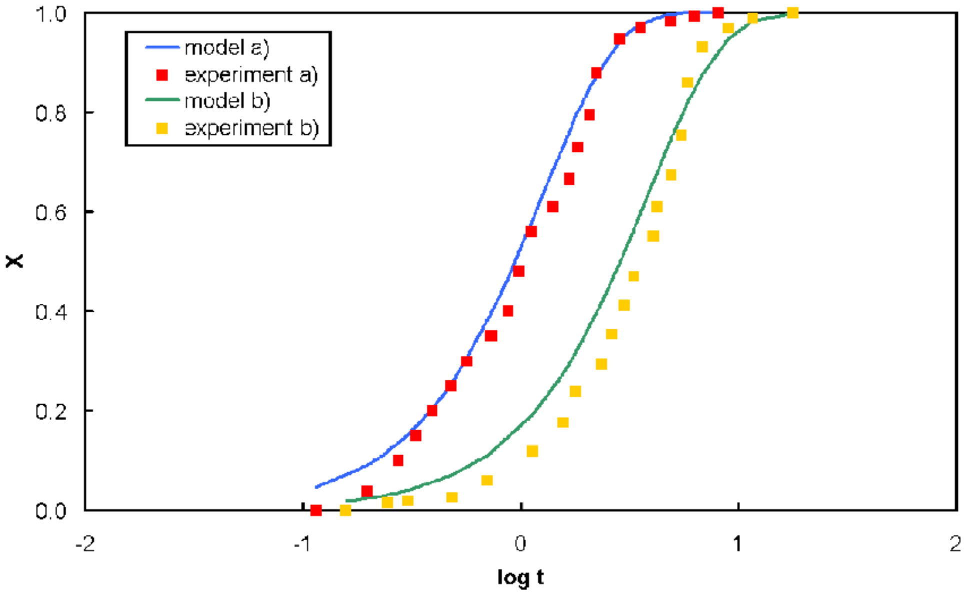

Figure 2.8 Fraction X calculated from experimental data plotted against the model prediction curves.

(M. Wang et al. 2008) successfully established a phase field model which simulates the microstructural evolution of recrystallization for the scale of micrometers and minutes. Figures 2.9 and 2.10 display the comparison between the studies experimental and simulated results. Grain boundary mobility is expressed in the form of Arrhenius formula. By fitting to experimental data, it is determined that the activation energy is the boundary segregation activity energy of the Zn atoms. The model proved to be in good agreement after comparing the simulated results to experimental results of the AZ31 alloy, which include temperatures ranging from 300°C to 400°C and recrystallization times up to 100 minutes. However, at 250°C results did not correlate well, which implies that between lower and higher temperatures there may be a mechanism variation in the activation energy.

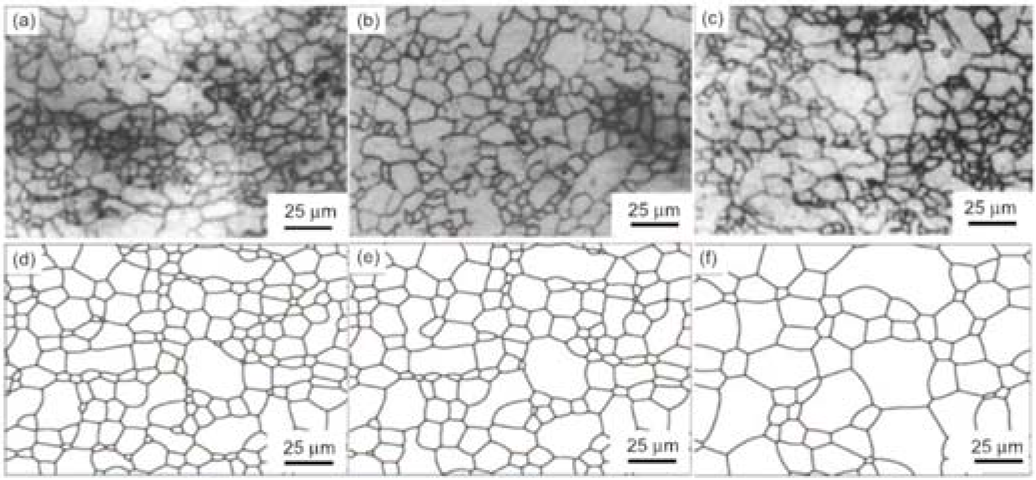

Figure 2.9 (a)-(c) the experimental photographs at 250C for 30min, 250C for 90min, 400C for 30min, respectively, (d)-(f) the simulations of the corresponding photographs.

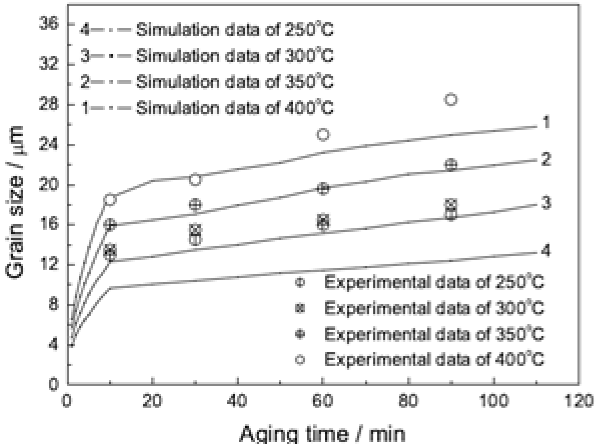

Figure 2.10 Simulated mean grain size evolution with time compared to experimental results.

(Prakash et al. 2009) investigated the deformation characteristics of magnesium using a crystal plasticity based finite element model (CPFEM) as well as morphological and crystallographic textures. The CPFEM offers advantages over the better known self consistent (SC) texture models. Because SC models such as VPSC fail to predict grain shape change, the shape is always limited to an ellipsoid which is insufficient. CPFEM also predicts the texture better, allowing for comparison with experimental results. It is concluded that the inhomogeneity of deformation during cold forming processes can greatly be attributed to the absence of pyramidal slip, which is typically thermally activated at temperatures greater than 200°C. It is also noted, that at lower temperatures twinning systems provide the deformation normal to the basal plane. However, twinning is accompanied by a large orientation change, usually very closely associated to that of the basal texture, limiting further deformation. Therefore, the deformation is substantially aided by the presence of the pyramidal slip system, which allows for deformation normal to the basal plane.

The effects of spatial stress distribution in an AZ31 sheet under in-plane compression are studied and simulated by (Choi et al. 2011). A complete 3-D CPFEM including crystallographic slip and deformation twinning is applied to simulate the spatial distribution of twin and slip that occurs during in plane compression of AZ31. To create a statistically representative 3-D microstructure, a microstructure mapping technique, which utilized EBSD to measure the grain size and microtexture, was utilized for the initial configuration. The crystallographic orientations obtained from EBSD data were assigned to the 3-D digital microstructure to match the experimental misorientation of the material. The CPFEM successfully captured the stress distribution, slip, and twin activities associated with the deformation of the material during in-plane compression.

(Walde & Riedel 2007) simulated the hot rolling of AZ31 and the texture evolution that accompanies the process. By incorporating crystallographic slip, twinning, and recrystallization into the visco-plastic self-consistent model, the main features observed in mechanical tests and in X-ray diffraction measurements of the texture are captured. The recrystallization texture model describes the hardening and softening behavior seen during hot compression of the alloy. Implementing the model into ABAQUS/Explicit, the hot rolling process is simulated, resulting in a predominant basal texture that is commonly observed in rolled Mg sheets. Including prismatic slip in the model is necessary to achieve the basal texture.

CHAPTER III

EXPERIMENTATION

3.1 Introduction

Samples of Magnesium alloy AZ31 are deformed at room temperature using a channel die apparatus. The deformed samples are then annealed at selected temperatures for a range of times to allow the microstructure to evolve. Attempting to capture the evolution of a material at the microstructural level requires careful and meticulous planning and preparation, leaving little room for error. This chapter describes the development and the execution of these experiments in detail.

3.2 Planning of Mechanical Testing

Because the material's microstructure is the topic of study, minimal alterations in how testing is performed can cause significant differences in how the samples ultimately evolve. The effects of deformation, strain rate, temperature, and initial texture on deformed AZ31 alloys have been studied by a number of researchers (Su et al. 2008), (Beer & M. Barnett 2008a),(Al-Samman & Gottstein 2008), and (Ulacia et al. 2010). It was concluded that alterations in these variables have an effect on the rate of evolution, grain growth, recrystallization, hardness, and activation of different deformation mechanisms. For this reason, the mechanical tests performed should be very concise and executed with precision. A slight difference in a sample's deformation or heat treating process could induce an evolution path different from the trend observed in other specimens. In this work, the specimens are deformed at room temperature and then annealed at high temperature to observe static recrystallization. To prevent premature fracture caused by a lack of slip systems at low temperatures, a lower strain rate of .001-s was chosen. The lack of formability of this alloy at ambient temperatures limits the options for sample deformation as well. However, strains around 6% are possible with well lubricated procedures. A deformation of 5% was chosen for this set of experiments because it has been established that for AZ31 and similar alloys, higher strains increase activation energy allowing for an enhanced grain growth rate and a lower recrystallization temperature (Su et al. 2008)(Winning & Schäfer 2006)(Volkert & Lingk 1998)(Wilkinson & Caceres 1984). Because the experimental deformation path is meant to approximate the material deformation during the rolling process, the channel die compression procedure was selected since it mimics the deformation conditions (plane strain compression) of material points at the center line of a rolled workpiece. The Instron uniaxial compression/tension testing machine is chosen to complete the testing configuration as the compression plates can be utilized to accommodate the channel die apparatus, and allow for easy sample placement and removal.

3.3 Methodology for Sample Preparation

As stated earlier, the mechanical testing methods used to alter the material are vital to its response and ultimately its final state. The effect of this is the need for very fluent and repeatable set of test methods. In order to keep the testing systematic, the samples must all be prepared and treated identically. The preparation methods of the samples for testing presented in a number of papers describing successful channel die compression tests were used to guide the formulation of the sample preparation methods for this study (Maurice et al. 2005)(Sediako et al. 2007)(Nave & M. R. Barnett

2004)(Raabe et al. 2001). All of these methods pay special attention to the reduction of friction factors as well as the sample fit to the channel die apparatus.

All samples were prepared from a 4mm thick rolled sheet of AZ31 (Mg-3%, Al-1%, Zn). The equipment used to prepare the samples is shown in Figure 3.1. Using a band saw, strips were cut from the sheet to a width of 14mm. The edges of the strips were milled down to create a smooth and uniform surface. Using a diamond saw, the samples were cut to a width of 5mm. Each sample was measured with a caliper after cutting to ensure the proper width. In previous studies, the corners and edges of the samples have proven to be points of maximum stresses among the samples due to higher friction values. Therefore, to aid in the reduction of friction, the samples edges were also slightly smoothed down as well. The equipment used in preparing the samples is displayed in Figure 3.1.

Figure 3.1 The machining tools used to prepare samples from the rolled sheet for channel die compression. From left to right: band saw, mill, diamond saw.

To minimize friction conditions during compression, samples were then prepared for deformation by wrapping them in a thin layer of Teflon tape and applying a conservative coat of polytetraflouroethylene (Teflon) powder with a cotton ball.

3.4 Channel Die Compression

After the samples are prepared, they were compressed using the channel die procedure. Figure 3.3 depicts the channel die compression setup. The channel die apparatus shown in Figure 3.2 is constructed out of stainless steel and contains a 5mm x 58mm channel which is used to restrain the sample during compression. The channel prevents expansion in the lateral direction, only allowing elongation of the sample along the length of the channel. Images of the channel die apparatus are provided in Figure 3.2.

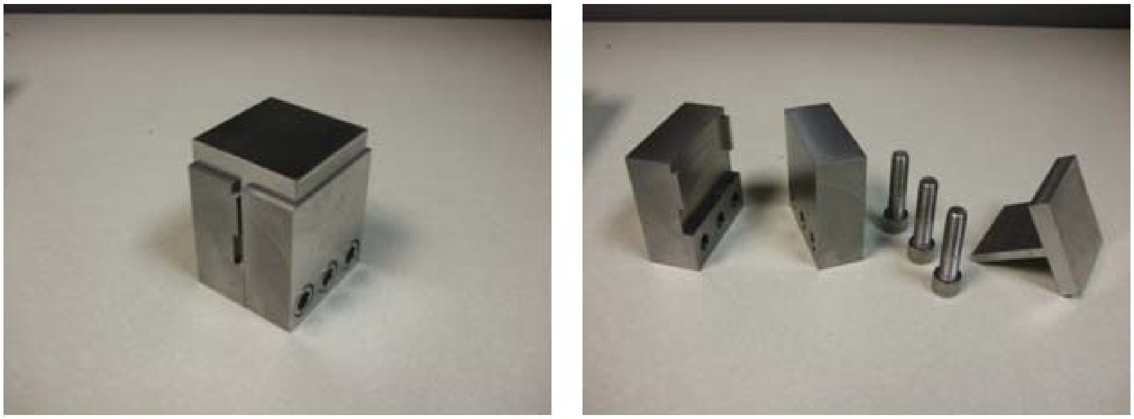

Figure 3.2 The image of the left represents the assembled channel die apparatus. On the right, an exploded view of the apparatus is displayed.

Using an Instron 5869 uniaxial tension and compression machine (see Fiugre 3.3), a sample reduction of 5% thickness from 4mm to 3.8 mm at a strain rate of $0.001s^{-1}$ was carried out for all samples. Two sets of compressions were performed. The first set of compressions allowed for elongation of the samples perpendicular to the rolling direction

(TD Samples) while the second set allowed for elongation along the rolling direction (RD Samples). The sample orientations, relative to the as received rolled sheet, are displayed in Figure 3.4.

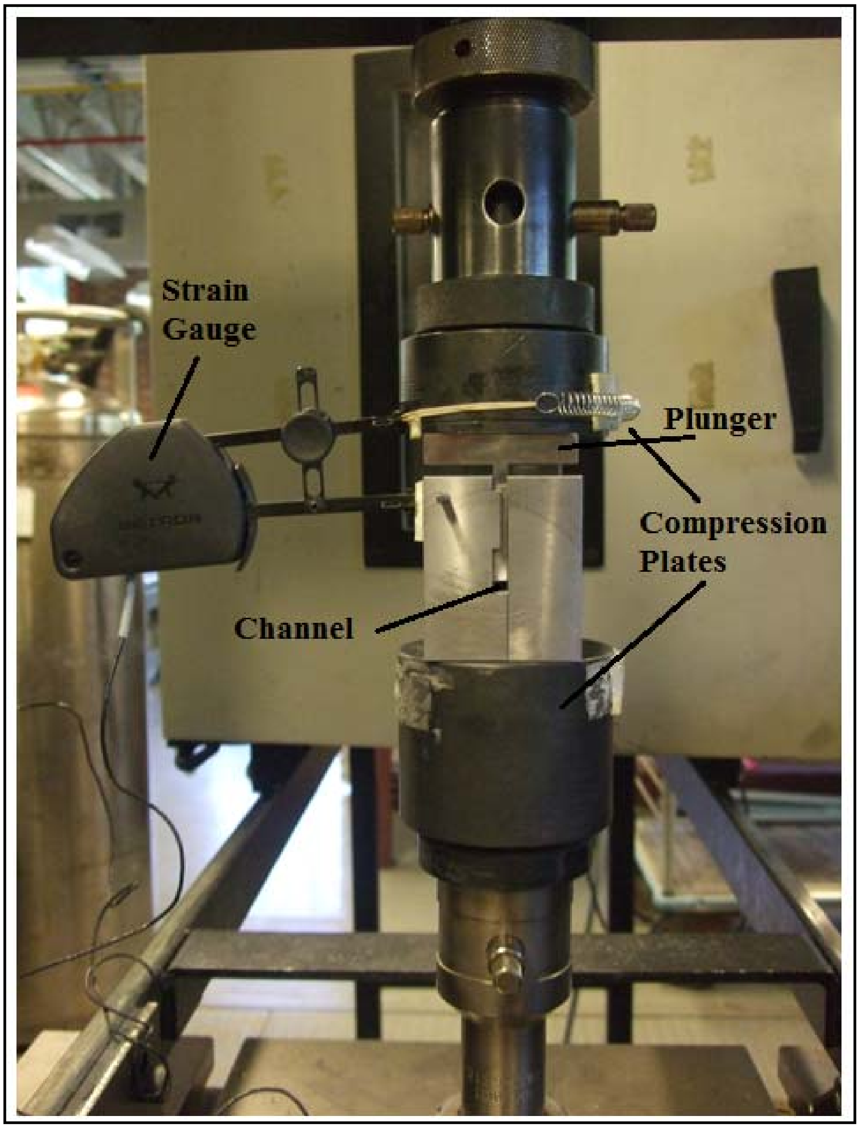

Figure 3.3 The channel die test apparatus setup.

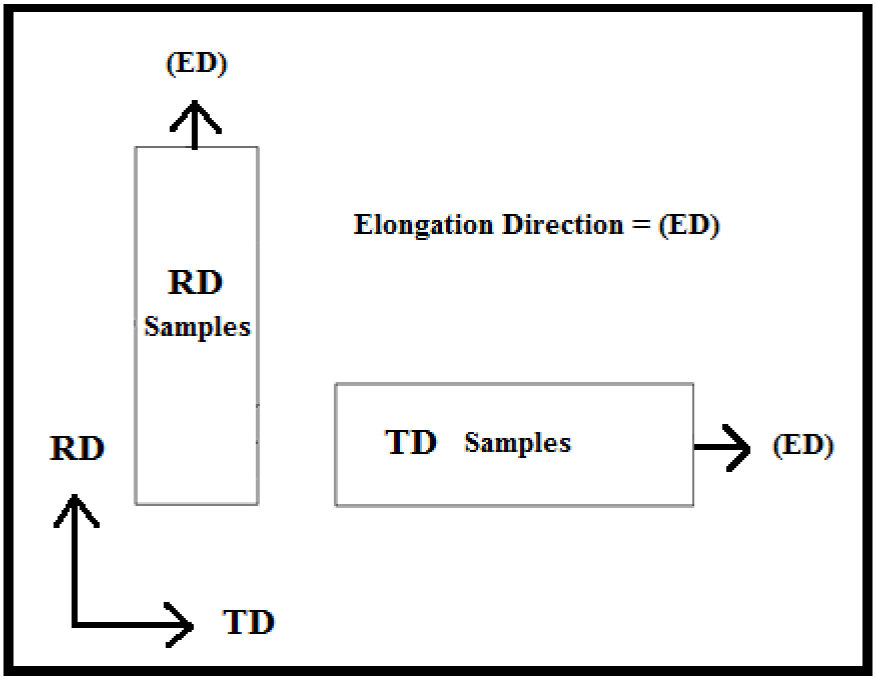

Figure 3.4 The image on the left represents how the RD samples are allowed to deform with respect to the original rolling direction of the sheet, while the image on the right represents that of the TD samples.

All of the samples were compressed along the c-axis, allowing for elongation in either the rolling direction (RD samples) or the transverse direction (TD samples). Magnesium alloys have proven to show a large amount of anisotropy, an aspect clearly depicted by the different response to expansion and compression along the c-axis. When comparing these two scenarios, there is a very noticeable difference in the stress strain curves. A study was performed by (Tucker et al. 2009) on the effects of material orientation to stress and strain, and the results are displayed in Figure 3.5.

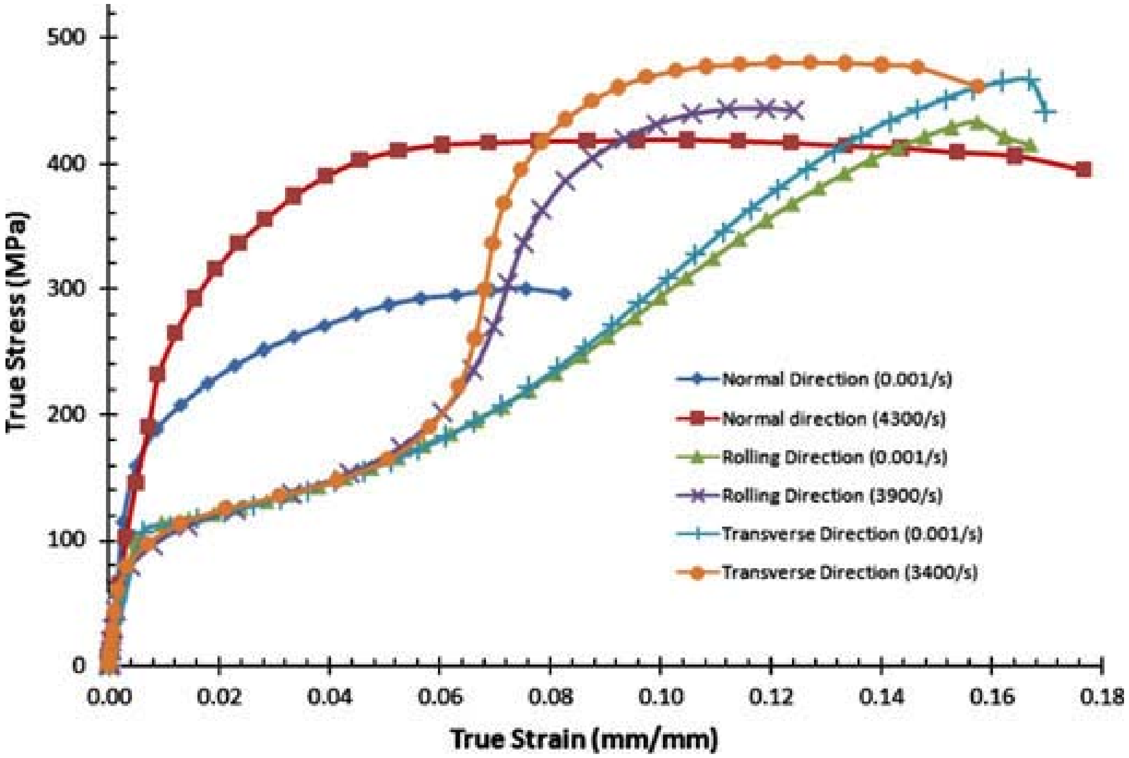

Figure 3.5 Compressive stress–strain behavior of AZ31B-H24 showingthe anisotropic effects on the strain rate dependence.

The difference in the curves compressed in the TD and the ND (along the c-axis) can be attributed to twinning and dislocations. Because compressing the material in the ND causes compression along the c-axis, twinning in the material is insignificant. Therefore, the ND curves only display the materials deformation due to dislocations. However, when viewing the curves representing samples compressed in the TD (allowing elongation along the c-axis), twinning is activated, and the curve is sigmoidal. Observation of the curves reveals that the material is loaded until twinning occurs. Once twinning is activated the material exhibits a large amount of deformation with respect to a small increase in stress. However, once the twinning is exhausted, the curve follows the same path as that of the ND samples. There is a large amount of loading with not much displacement until the dislocation region is activated, resulting in the same curve pattern as the samples compressed in the ND.

Since all of the samples compressed in this study are promoting compression of the material along the c-axis, it can be expected that the force vs displacement curves for the TD and RD samples should be very similar, as shown in Figure 3.6. The curves are a representation of what is occurring in the materials microstructure as far as energy needed to cause dislocation and deformation of the material. Although compression of the RD and TD samples reveal similar curves, the question still remains as to what the microstructure looks like for the two scenarios. The RD samples are allowing for further elongation of the initially rolled grains, while the TD samples should promote elongation of the grains perpendicular to the as received rolled sheet of AZ31.

For the study, a total of 42 samples were compressed in the channel die fixture (25 TD samples and 17 RD samples) at room temperature and at a strain rate of 0.001 s^{-1} to a strain of 5%, as shown in Table 3.1. A comparison of the Force vs. Displacement data for the two sets of samples is also provided in Figure 3.6.

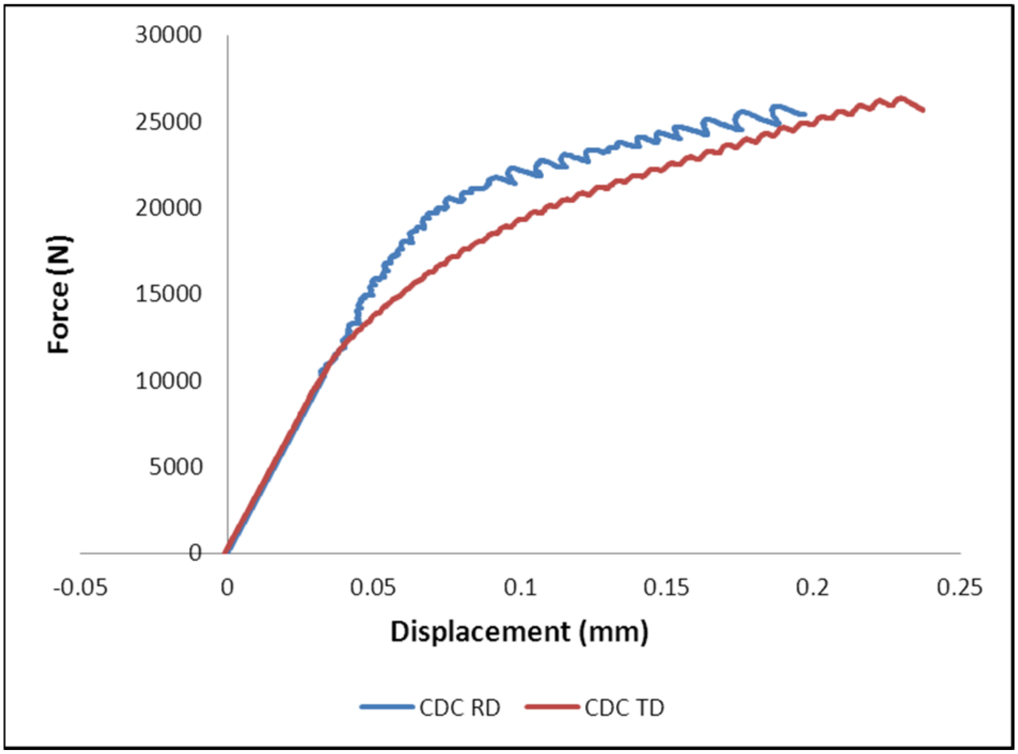

Figure 3.6 Force vs. Displacement curves for the RD and TD samples.

Table 3.1 Test Matrix for Channel Die Compression Tests

	RD Samples	**TD Samples**
Compression Method	Channel Die Compression	Channel Die Compression
Temperature	Ambient	Ambient
Strain Rate	$0.001s^{-1}$	$0.001s^{-1}$
Deformation	5%	5%
Number of Samples	17	25

3.5 The Annealing Process

Heat treating of the samples was performed subsequent to deformation. In the attempt to capture the specimens' microstructural states at different points in the process, a series of annealing times were selected ranging from 10s to 10,000s. Temperature effects are also of interest since it has been demonstrated that increasing temperatures can cause a more rapid recovery (Su et al. 2008)(Beer & M. Barnett 2008b)(Volkert & Lingk

1998). To gain an understanding of how the material responds to these changes, several temperatures, common to industrial application, were selected (375°C, 400°C, and 425°C). The samples were annealed in a carbolite tube furnace for the specified annealing times and temperatures, as shown in Figure 3.7 and Tables 3.2 and 3.3

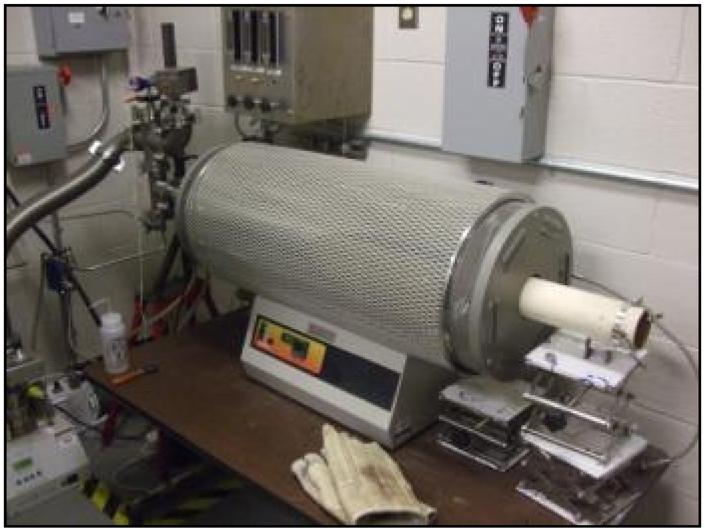

Figure 3.7 Image of the carbolite tube furnace used to anneal samples at the specified times and temperatures. Samples are inserted and extracted through the tube extruding from the right portion of the furnace.

Upon the removal of each sample, the specimens were quenched to prevent the further evolution of their microstructures. This allowed for a step by step inspection of the material's response at the chosen stages throughout the annealing process.

Table 3.2 The selected annealing times and temperatures for the TD samples.

TD Samples

Temperature (^oC)	Annealing Time (seconds)							
375	10	50	250	500	1,000	2,500	5,000	10,000
400	10	50	250	500	1,000	2,500	5,000	10,000
425	10	50	250	500	1,000	2,500	5,000	10,000

Table 3.3 The selected annealing times and temperatures for the RD samples.

RD Samples

Temperature (^oC)	Annealing Time (seconds)							
375	10	50	250	500	1,000	2,500	5,000	10,000
425	10	50	250	500	1,000	2,500	5,000	10,000

CHAPTER IV

DATA COLLECTION METHODS

4.1 Introduction

In order to achieve the goals of the study, data was collected and analyzed, utilizing several techniques such as microhardness testing, optical microscopy, and electron backscattering diffraction. These methods were chosen because they have proven to provide the information needed to quantify the material's microstructural changes induced by deformation and heat treatment. Utilizing the selected methods allowed for a characterization of the microstructure evolution both visually and numerically.

4.2 Mounting and Polishing Techniques

After the samples were completely subjected to deformation and heat treatment, they were prepared for assessment. For many of the observation and data acquisition methods used, a sample mount was required. There are two typical mounting techniques. Hot mounting and cold mounting. Because one of the points of the study was to observe the materials reaction to heat, the samples were cold mounted to avoid any further evolution of the microstructure due to heat. An epoxy resin was mixed with a hardening reagent to create the cold mount mixture. The sample was placed in a plastic mold and the mixture was applied using the Struers cold mounting machine, see Figure 4.1.

Figure 4.1 Image of the Struers equipment used to cold mount the samples. A vacuum is created inside of the chamber to apply the resin mixture and prevent bubbles (bubbles in the mount can lead to trapped grit later in the polishing stages).

Once the samples were mounted, polishing was required at various levels throughout the analysis process. The polishing procedures were carried out using Struers polishing machines, represented in Figure 4.2. Two separate polishers were used. For the first polishing stages, the polisher capable of larger rotational speeds was used. However, once the samples reached the final stage of polishing, the polisher with lower rotational speeds was used to prevent damage to the sample surface.

Figure 4.2 The Polishing equipment utilized to prepare samples for analysis. The image on the left represents the Struers LaboPol-11. This is used for the first four steps in polishing. The machine on the right is the Struers LaboPol-4, and it is used in the final stage of polishing.

Before testing the samples hardness, the samples were polished to the fourth step of the Mg- preparation process provided in Appendix A. The sixth step of polishing described in Appendix A was used after hardness testing to prepare the sample surface for both Optical microscopy and Electron Backscattering Diffraction studies. The polishing procedure caused slight deformation of the top layer of the material surface. Therefore, etching was used to remove this deformed layer and provided an enhanced material surface for observation. Two separate etchants were used. The application of Picric acid allows for a very visible grain structure. Therefore, it was applied to the samples prior to optical imaging. Acetic acid proves to aid in the quality of crystallographic patterns. Hence, it was applied to the samples prior to EBSD scanning.

4.3 Vickers Microhardness

In previous studies, a material's hardness has successfully been used to calculate a number of mechanical properties. The focus of this work is to predict the recrystallized fraction of AZ31 using experimental hardness values (Su et al. 2008)(Beer & M. Barnett 2008b)(Chao et al. 2011). It is important to note that the hardness data not only allows for the calculation of the sample's fraction of recrystallization, but it also provides data that illustrates the softening that occurs in the material due to an increase in the annealing time and temperature. The mechanics that cause the softening phenomena will be discussed in more detail in chapter V.

After a brief polishing of the sample surfaces, the microhardness tests were carried out using a Vickers hardness tester with a 50g force, see Figure 4.3. Five indentation readings were collected at different points on the sample surface and averaged to prevent skewed data that may occur from any localized grain structures within the sample.

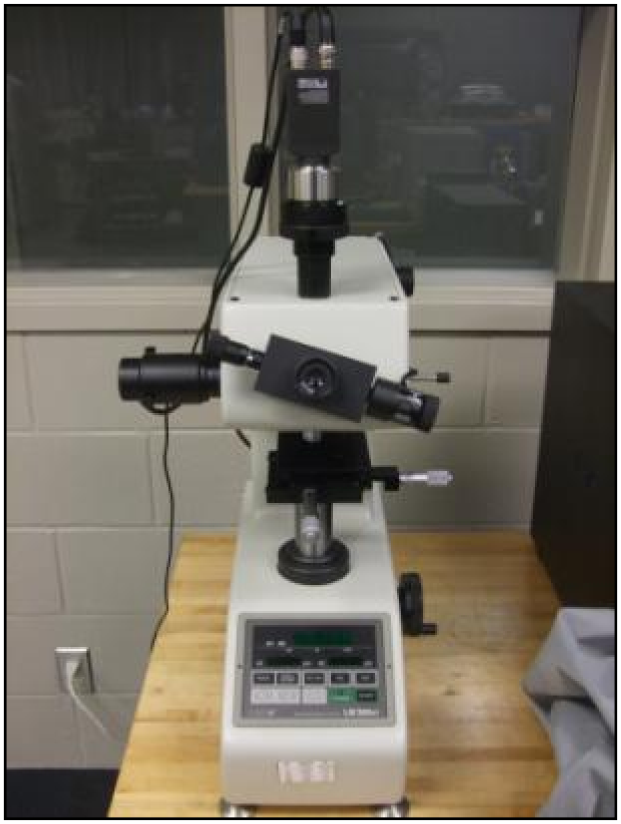

Figure 4.3 The Microhardness indentor used to gather hardness data of the deformed and annealed samples.

4.4 Optical Microscopy

Optical images are used frequently in microstructural studies for several reasons. Imaging allows for a relatively fast and reliable method for determining grain evolution. The visual representation of optical microscopy, not only depicts the physical change in the evolving microstructure of the material (such as grain nucleation and growth), but the images can be used to collect grain size data as well. Many publishers use optical imaging to verify changes in microstructure due to temperature, stress, strain, and strain rate (Su et al. 2008)(Beer & M. Barnett 2008b)(Winning & Schäfer 2006).

For the best results, all samples were completely polished using the method described in appendix A. Just prior to optical imaging, the samples were etched in a picric acid. This solution provides a suitable grain structure for viewing under the microscope. The sample images were captured using the Zeiss Optical Microscope, see Figure 4.4, and the Zeiss image software. Images are collected from the sample surfaces at multiple magnifications for the samples selected.

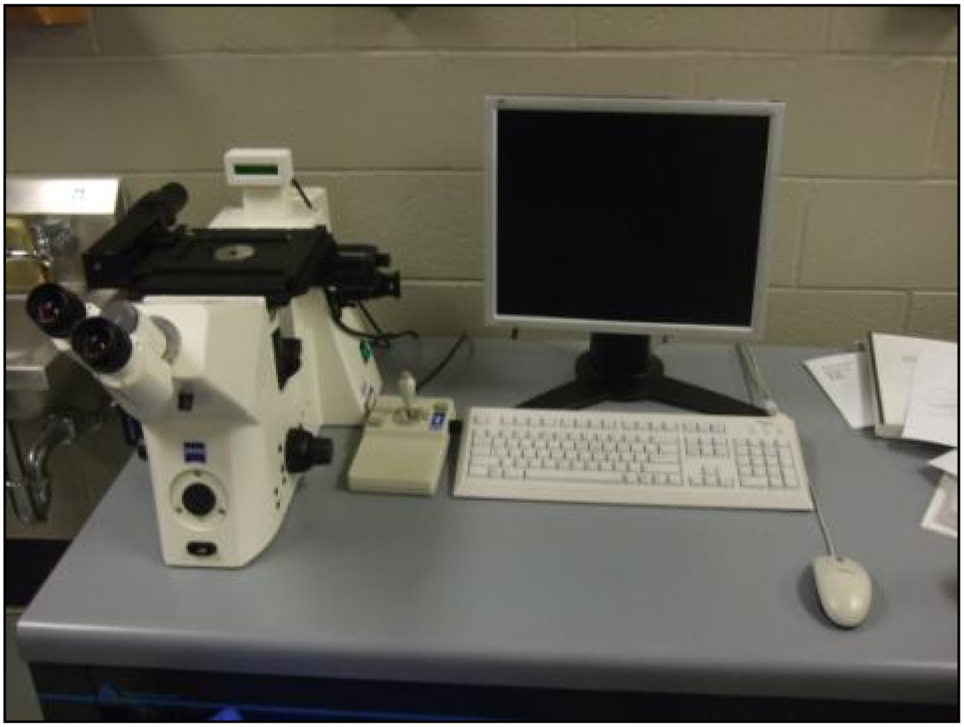

Figure 4.4 Image displaying the system used for optical microscopy. The system includes a Zeiss optical microscope (on the left) and Zeiss image analysis software on the computer represented on the right.

4.5 Electron Backscatter Diffraction (EBSD)

Electron Backscatter Diffraction, better known as EBSD, is becoming a more exploited method of collecting and analyzing material data. With an increasing understanding for the process, EBSD has become a reliable way of collecting multiple types of data with just one scan. The equipment used for this work is shown in Figure 4.5. Different EBSD analysis techniques have been investigated and compared to hardness measurements for the use of EBSD in characterizing recrystallization fraction. It is concluded that the misorientation based methods provide the most reliable results (Dziaszyk et al. 2010). The concept for these methods is that the deformed unrecrystallized material contains large amounts of dislocation and misorientation; therefore, portions of the material with low misorientations are classified as recrystallized. Methods such as Kernal Average Misorientation, Grain Orientation Spread, and Grain Average Misorientation all utilize this concept (Mccabe & Teter 2006)(Jain et al. 2006)(Dingley 2004)(Lu et al. 2003). Several studies also explore the use of high angle grain boundary (HAGB) data obtained from EBSD as a tool for acquiring the fraction of recrystallized material. The HABG % proves to increase significantly with temperature during annealing when recrystallization occurs (Jazaeri & F. Humphreys 2004). Measuring the fractional changes of these HAGBs can be used to measure the percentage of recrystallization (Rex%) in 20% of the time it takes to perform line analysis of area maps. However, it has been observed that the HAGB method is not useful in materials that display continuous recrystallization kinetics. For the continuous recrystallization process, it has been found that the HAGBs do not evolve much after reaching 60-70%.

Performing EBSD requires a scanning electron microscope and data analysis software. The equipment utilized in this study is displayed in Figure 4.5.

Figure 4.5 The FEG scanning electron microscope is represented on the left. The picture on the right represents the entire setup: FEG SEM, SEM control software, and the OIM data collection software from left to right respectively.

CHAPTER V

DATA ANALYSIS AND INTERPRETATION

5.1 Introduction

The methods described in chapter IV provided the necessary data depicting how the material's internal structure transforms. In this chapter the collected data from hardness tests, optical microscopy and EBSD is presented and analyzed to describe the material's microstructure evolution during the annealing process. At the same time, the material hardness and microstructure information is used to help illustrate how static recrystallization occurs in AZ31. Results clearly show that the internal structure of the material is altered by annealing time and temperature.

5.2 Microhardness

Following the Vickers hardness testing methods described in chapter IV, several hardness readings were recorded for each sample. The average hardness values were then used to create a graphical representation of the evolving hardness of the material during the annealing process. The hardness data collected for samples in both the TD and RD are represented in Tables 5.1-5.6. The hardness value for the as-received material is recorded as well. The average hardness value of the as-received material is measured to be 64 HV. This value is much lower than the hardness values of the deformed RD and TD samples prior to annealing. Average hardness values for the RD and TD specimens were measured as well and were recorded as 78HV and 76HV respectively.

Original Hardness: 64HV RD Hardness: 78HV TD Hardness 76 HV

Table 5.1 Hardness data for TD samples annealed at 375°C.

Seconds:			**HV @ 375°C**			**AVG:**
10	69	78	76	77	76	**75.2**
50	70	70	73	69	73	**71**
250	70	74	75	69	72	**72**
500	68	74	68	69	71	**70**
1000	73	69	69	67	65	**68.6**
2500	64	69	71	69	70	**68.6**
5000	67	65	69	70	71	**68.4**
10000	63	71	70	67	63	**66.8**

Table 5.2 Hardness data for TD samples annealed at 400°C.

Seconds:			**HV @ 400°C**			**AVG:**
10	71	75	75	72	70	**72.6**
50	69	69	70	67	70	**69**
250	70	72	71	73	69	**71**
500	68	62	62	72	72	**67.2**
1000	70	71	69	70	71	**70.2**
2500	71	69	64	67	69	**68**
5000	66	68	66	67	67	**66.8**
10000	72	62	68	60	65	**65.4**

Table 5.3 Hardness data for TD samples annealed at 425°C.

Seconds:			**HV @ 425°C**			**AVG:**
10	75	68	76	71	69	**71.8**
50	70	69	69	69	67	**68.8**
250	70	69	68	70	65	**68.4**
500	69	62	68	62	72	**66.6**
1000	68	65	66	67	70	**67.2**
2500	66	68	69	70	61	**66.8**
5000	64	64	66	68	67	**65.8**
10000	65	65	62	68	66	**65.2**

Table 5.4 Hardness data for RD samples annealed at 375°C.

Seconds:			<u>**HV @ 375°C**</u>			**AVG:**
10	79	78	78	76	75	**77.2**
50	74	72	73	72	74	**73**
250	70	71	72	70	71	**70.8**
500	73	71	72	71	70	**71.4**
1000	72	69	68	71	70	**70**
2500	71	69	71	68	67	**69.2**
5000	65	68	69	70	70	**68.4**
10000	66	65	67	69	68	**67**

Table 5.5 Hardness data for RD samples annealed at 425°C.

Seconds:			<u>**HV @ 425°C**</u>			**AVG:**
10	79	75	76	76	75	**76.2**
50	75	74	75	77	76	**75.4**
250	70	71	70	72	72	**71**
500	69	70	68	69	71	**69.4**
1000	71	69	67	68	70	**69**
2500	69	66	67	68	68	**67.6**
5000	65	67	66	67	66	**66.2**
10000	66	65	66	66	65	**65.6**

5.2.1 Material Hardness Evolution

It has been observed that a material’s hardness decreases at a faster rate due to increasing temperatures and strains. A graph displaying the hardness evolution of an AZ31 alloy, which was subjected to similar conditions as the alloy in this study, is provided in Figure 5.1 (Su et al. 2008). (Jain et al. 2006) has also shown that larger deformations provide for a faster rate of change of the materials hardness as the annealing time is increased.

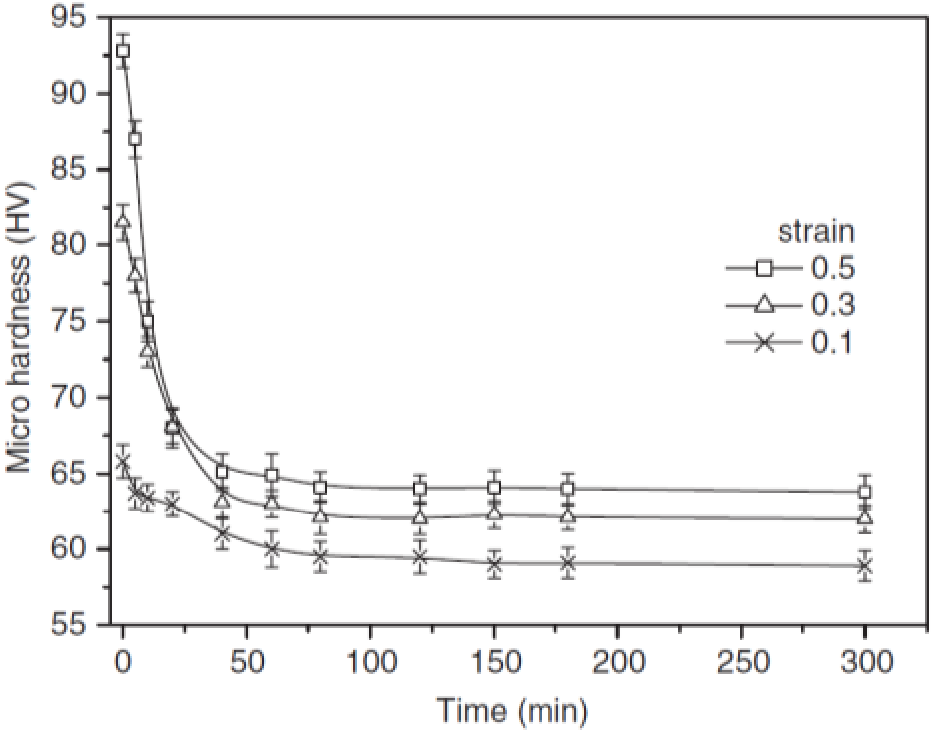

Figure 5.1 Microhardness evolution of cold deformed AZ31 due to annealing time for several strains.

Similarly to what is observed in changes in hardness due to strain and strain rate, changes in the materials hardness due to temperature should display a similar trend, Figure 5.2 displays the results of the hardness values obtained for the TD samples. As expected, hardness decreases at an increased rate for samples annealed at higher temperatures. The hardness of the as received material is measured at 64HV while the hardness of the deformed sample after plane strain compression and before annealing is measured to be 76HV. Clearly, the hardness of the material at this state is much higher than that of the as received material, which is to be expected. As the original material is compressed, energy is applied to the material and trapped in the microstructure as dislocations and other internal energies. The cold deformation of the material results in cold worked samples which internally causes work hardening of the material with the consequent increase in hardness.

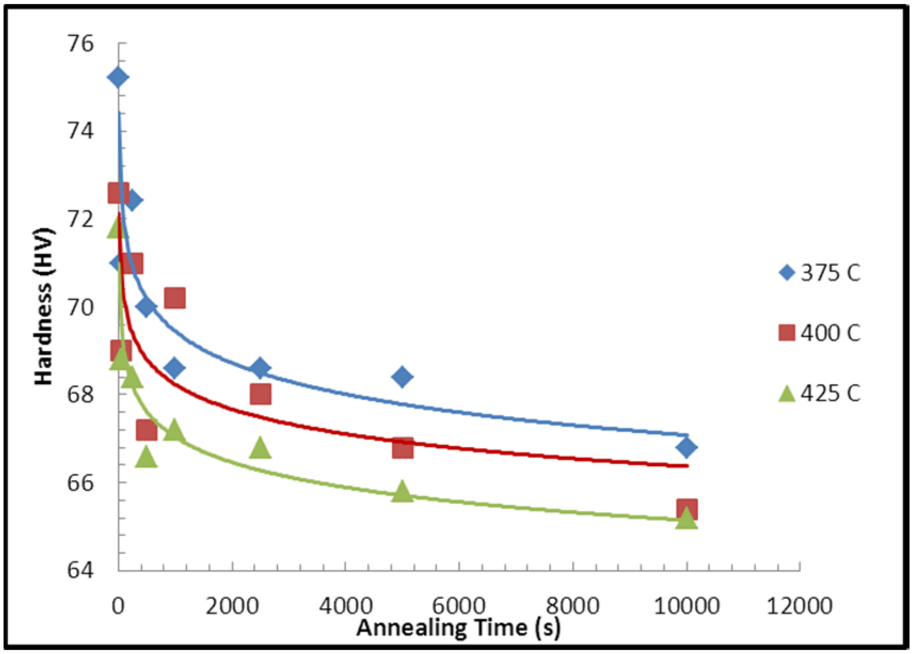

Figure 5.2 Microhardness evolution of the TD AZ31 samples at 375°C, 400°C, and 425°C.

Specifically, Figure 5.2 shows the hardness evolution for the samples annealed at 375°C, 400°C, and 425°C. The samples were annealed for times ranging from 10 – 10,000 seconds. It is evident that the majority of change occurs in the first 500 seconds. After this time the hardness seems to gradually decrease for all temperatures. Temperature is known to have the greatest effect on recrystallization kinetics. When observing the trends of the change in hardness, it is evident that temperature affects the materials hardness evolution as well. Higher temperatures cause a larger decrease in hardness at earlier than that of the lower temperatures. Also, it is revealed that increased temperature results in a lower final hardness as well. Similar explanations of what is occurring with the materials hardness are displayed in Figure 5.3. This figure reveals the substantial effect that temperature and annealing time have on the material. It is evident from comparing several annealing times at the same temperature that as the annealing time increases, the materials hardness decreases. It is suggested that the longer annealing times allow for a more homogeneous grain structure to evolve, resulting in a softer material with larger grains. A comparison can also be made about the same annealing time at the different temperatures. Tracking the hardness value of one annealing time reveals that the temperature has a profound effect on the hardness. The hardness values of the samples annealed at higher temperatures consistently provide a lower hardness values than the samples at lower temperatures.

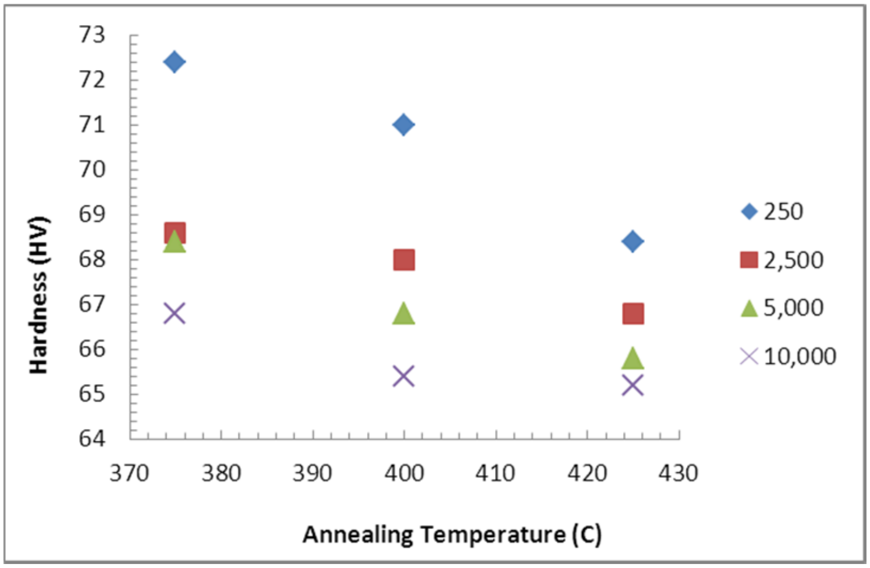

Figure 5.3 Comparison of Hardness for TD samples annealed for 250, 2500, 5000, and 10000 seconds for temperatures of 375°C, 400°C, and 425°C.

Similarly to the TD samples, samples allowed to elongate during compression in the rolling direction (RD samples), were tested for their hardness values. The results are very similar. It appears that much of the change in material hardness occurs in the early stages of the annealing process, a trend resulting in rapid change during the early stages, followed by gradual decrease. The trends for the change in hardness for the RD samples are displayed in Figure 5.4. The materials hardness seems to react in a common manner for the two sets of samples.

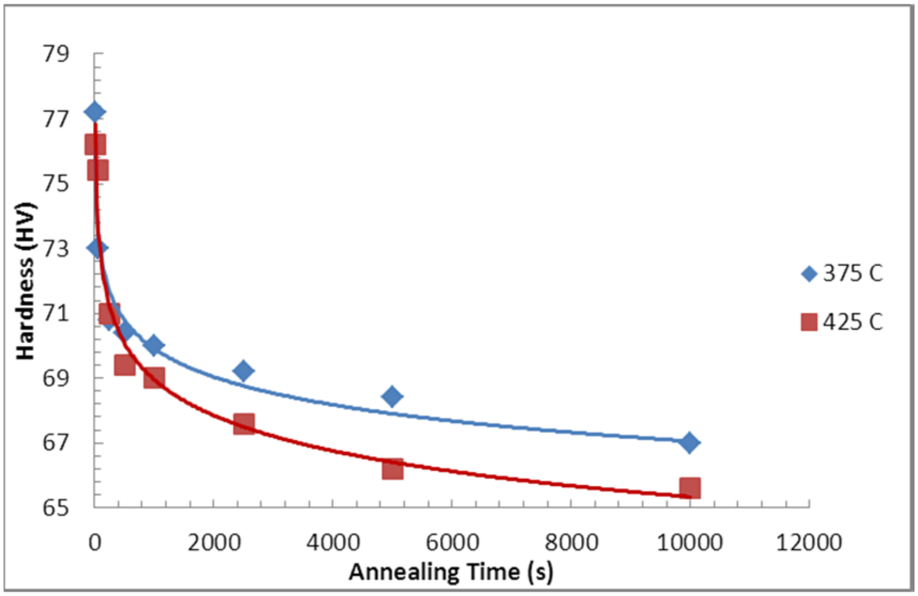

Figure 5.4 Microhardness evolution of the RD AZ31 samples annealed at 375°C and 425°C.

In magnesium samples compressed along the c-axis and allowed to expand in the RD and TD directions, it has been established that only a small difference will be seen among the stress strain curves. However, since RD samples are allowed to elongate parallel to the rolling direction and since TD samples are allowed to elongate perpendicular to the rolling direction, the microstructures could vary within the two sets of samples. For this reason, a comparison of the microhardness evolution of the two sets of specimens is made. Figure 5.5 compares the RD and TD samples annealed at a temperature of 375°C and Figure 5.6 compares the two sets at 425°C.

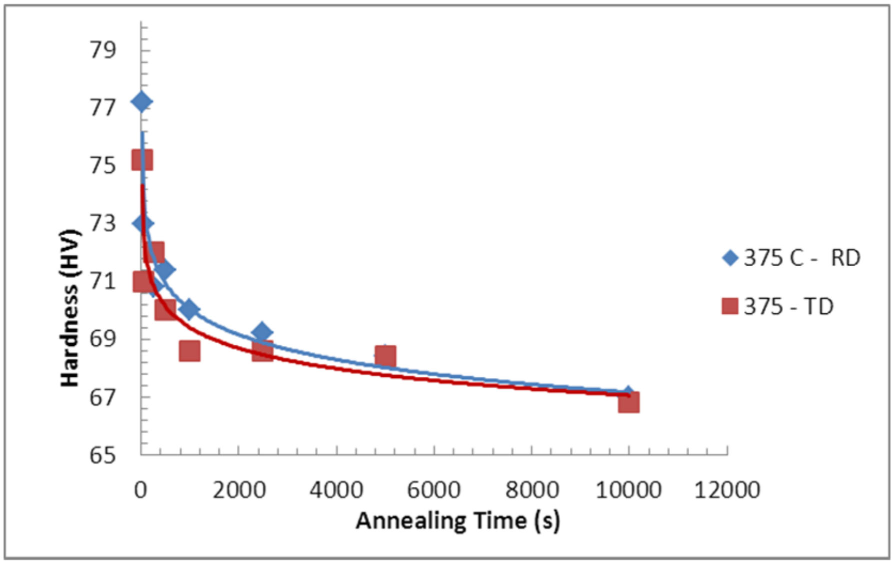

Figure 5.5 Comparison of the microhardness evolution of RD and TD samples annealed at 375°C.

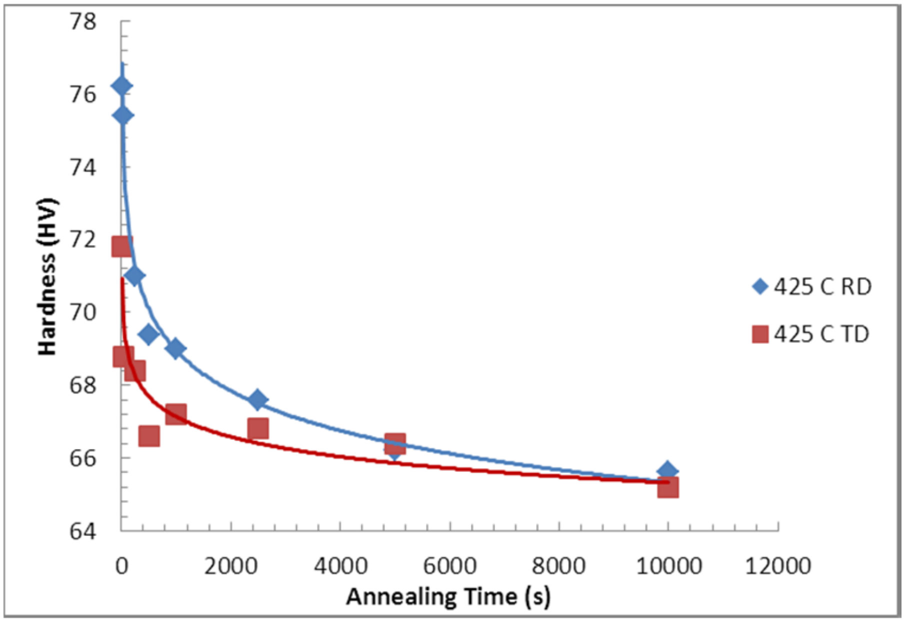

Figure 5.6 Comparison of the microhardness evolution of RD and TD samples annealed at 425°C.

Comparing the two sets of samples reveals that the different orientation of the samples has little effect on the hardness evolution for the samples annealed at 375°C.

The hardness of the RD samples seems to be slightly less than that of the TD samples at this temperature. However, at 425°C the evolution of the two sets seems to deviate more. It seems that the TD samples decrease in hardness value at a faster rate. Although some variation is seen at the beginning of the annealing process, the hardness values of the samples at both 375°C and 425°C seem to converge at later times, resulting in very similar final hardness values.

5.3 Relative Change In Hardness

To better compare the hardness evolution presented in the previous section for different temperatures, the relative change in hardness can be plotted against time. The relative change in hardness shows the trend for the rate of recrystallization and can be defined by the following equation:

$$\Delta H = \frac{Hmax - HT}{Hmax - Hmin} \tag{5.1}$$

ΔH – relative change in hardness
Hmax – Hardness of as-deformed material
HT – Hardness of Partially recrystallized material
Hmin – Hardness of Fully recrystallized material

(Su et al. 2008) Performed a similar study on AZ31 billets compressed at room temperature. The results from this study, shown in Figure 5.7, reveal that at higher temperatures, the rate of hardness evolution is significantly increased.

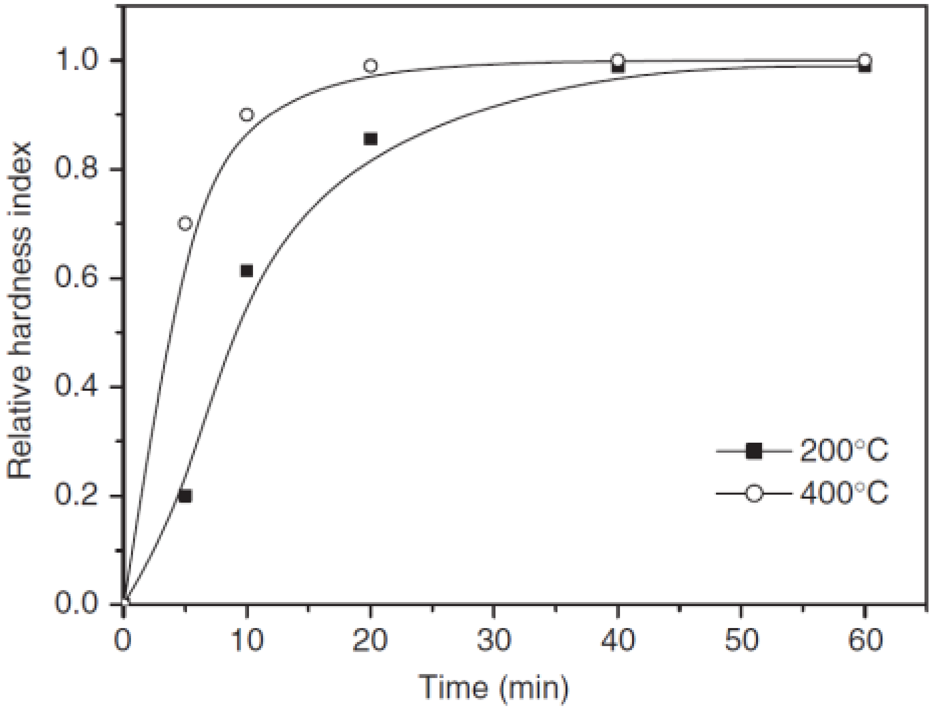

Figure 5.7 Relative Hardness of samples at strain of ε = 0.5 and temperatures of at 200°C and 400°C.

Similarly to (Su et al. 2008), the results from hardness testing were converted into relative hardness values for selected times. The relative hardness values are displayed numerically in Tables 5.6 and 5.7 for the TD and RD samples respectively.

Table 5.6 Relative hardness values calculated for the TD samples.

	0s	**10s**	**250s**	**500s**	**5000s**	**10000s**
375°C	0	0.087	0.391	0.652	0.8261	1
400°C	0	0.32	0.4717	0.8302	0.868	1
425°C	0	0.389	0.704	0.8704	0.944	1

Table 5.7 Relative hardness values calculated for the RD samples.

	0s	**10s**	**500s**	**2500s**	**5000s**	**10000s**
375°C	0	0.073	0.6	0.8	0.873	1
425°C	0	0.145	0.6935	0.8387	0.9516	1

Figures 5.8 and 5.9 display the trends of the relative change in hardness for TD and RD samples respectively. In both figures, the change in relative hardness demonstrates a rapidly increasing trend followed by a gradual increase. This trend is seen for all temperatures and in both the TD and RD samples. It is clear that increasing the annealing temperature results in an increased rate of hardness evolution. This suggests that the higher temperatures are activating the recrystallization process in the material earlier at an increased rate of recrystallization.

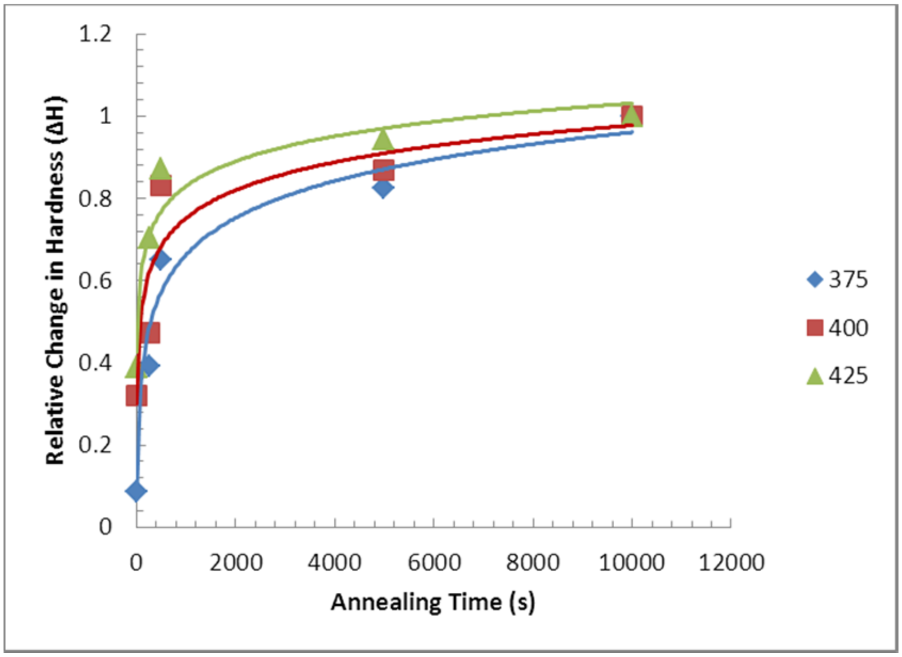

Figure 5.8 Comparison of relative hardness curves for the TD samples.

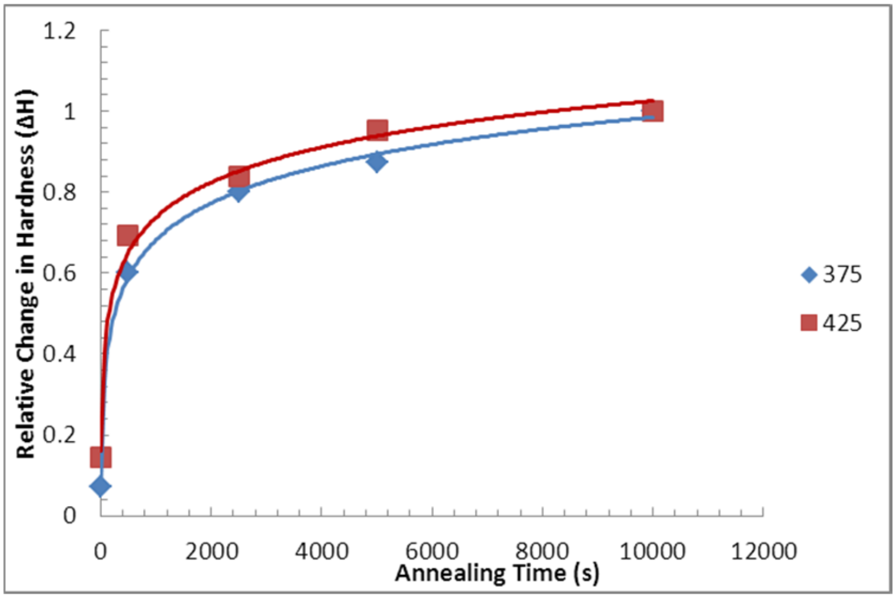

Figure 5.9 Comparison of the relative hardness curves for the RD samples.

5.4 Optical Microscopy

In order to gain a visual understanding of how the microstructure is evolving throughout this process, optical images are taken at certain reference points. These points along the material's evolutionary path are selected beginning with the as received material and conclude with the final annealing time of 10,000 seconds. To begin to understand how the materials microstructure is changing, the microstructure of the as received material must be observed. Figure 5.10 displays the as received material, or a rolled sheet. In general, plastic deformation caused by the rolling process significantly increases the strength. The microstructures of rolled alloys typically display a large number of twins and shear zones. These twins appear either perpendicular or deviated from the rolling direction. The twinning in Mg alloys may partially accommodate the plastic strain induced by rolling, and can be an important deformation mode which can allow the material to react more ductile than brittle. The twinning zones do not only aid in the deformation process, but are very significant in the microstructural evolution of the material as well. Twins present after rolling play an important role during the annealing process due to their accumulated energy. Twins are very often the site for the nucleation of new grains, a process vital to the recrystallization of the material.

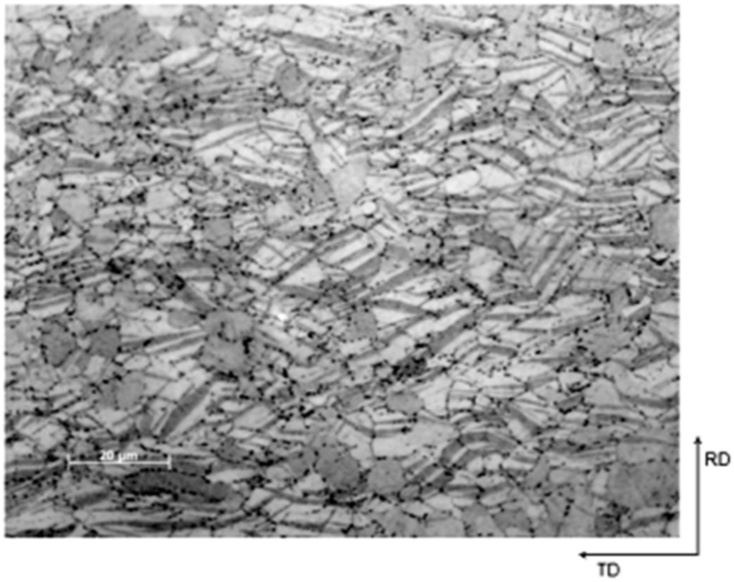

Figure 5.10 Optical image of the as-recieved AZ31 sheet microstructure.

As expected, the microstructure of the as received material reveals large amounts of deformation and twins. The rolling direction is vertical, and it is evident that the twins appear perpendicular to the rolling direction. The grain structure of the as received material appears to be highly disorganized, and only a small portion of the grains do not appear to contain some type of dislocation or twinning. Figures 5.11 and 5.12 display the microstructures of the as-deformed RD and TD specimens, respectively. Recall that not much difference is seen in the Force vs. Displacement curves for the two sets of samples. However, the RD samples required slightly more force to deform, and a slightly decreased rate of softening was observed in the RD samples as well. Therefore, an inspection of the two microstructures at this stage is important to see if any differences can be observed. Comparing the two microstructures does not reveal any severe differences. However, several distinctions can be noted. The RD sample reveals a more nonhomogeneous microstructure across the entire sample surface. The majority of the sample surface contains areas of increased dislocation and twinning, while smaller regions of somewhat defined grain structure can be seen. In contrast, the TD sample displays a more evenly distributed microstructure consisting of a constant amount of twinning and dislocation spanning the entire sample surface.

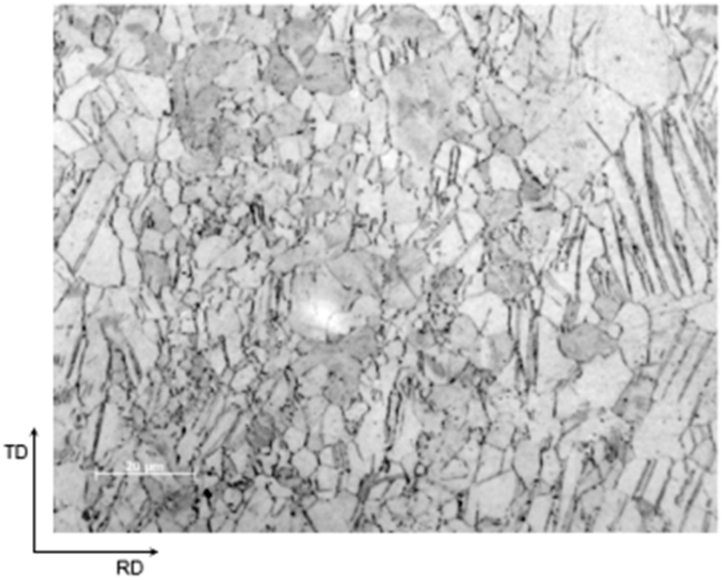

Figure 5.11 Optical image of the RD sample after compression and before annealing.

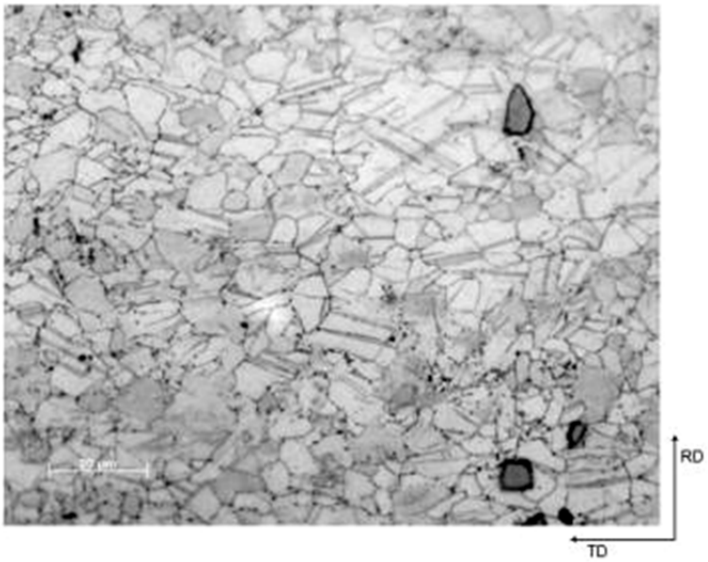

Figure 5.12 Optical image of the TD sample after compression before annealing.

5.4.1 The Microstructural Evolution of AZ31

During the annealing process, the material's microstructure will evolve. The deformed and annealed samples undergo the recovery and recrystallization processes. Through the recovery process, dislocations rearrange into lower energy configurations. The recovery stage is detected by the decrease in hardness from the as-deformed state and before the microstructure begins to show the nucleation of recrystallized grains. This process usually results in the formation of subgrain boundaries. However, since both the recovery and recrystallization processes are driven by stored energy, the distinction between the two processes is very difficult to quantify and capture using optical microscopy. Typically, the recovery process is labeled as the region where decrease in hardness occurs until the first nucleation of a new grain occurs, thus signifying the onset of recrystallization, which is said to be complete at the last formation of a new grain.

The evolution of the microstructure for the TD samples was captured using optical microscopy, as well as images from the EBSD scans. The optical images are presented in Figure 5.13, and display the microstructure of samples annealed for 10s, 1000s, and 10000s for all three temperatures. Similarly, Figure 5.14 provides images obtained from EBSD of the microstructures at all three temperatures for samples annealed at 50s, 1000s, and 10000s. Although the images are obtained using different methods, the two figures provide very similar results.

TD Samples

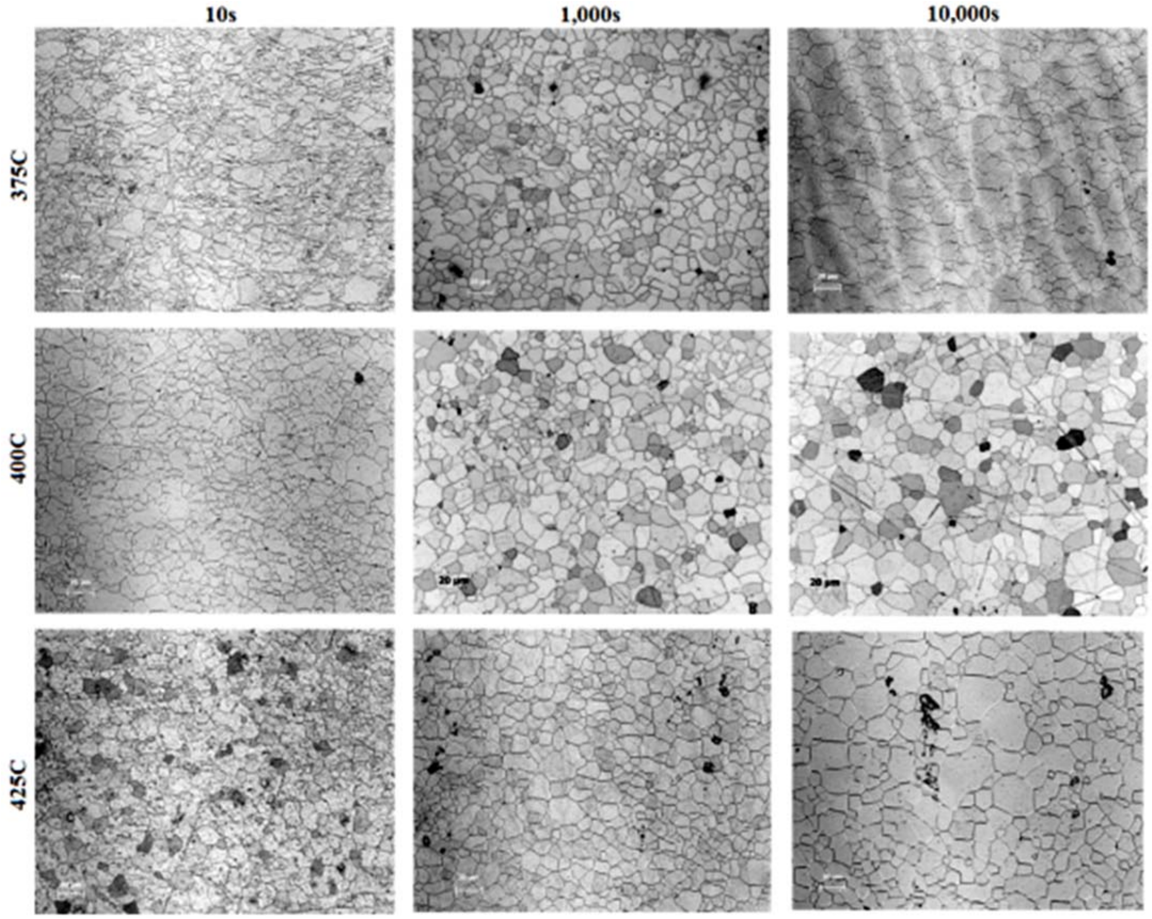

Figure 5.13 The microstructural evolution of the TD samples after annealing at 375°C, 400°C, 425°C for 10s, 1000s, and 1000s.

When observing the microstructures of the annealed samples, the appearance of new grains can only clearly be seen for samples annealed at 10s. Once the samples have been annealed for 50s, it is hard to differentiate between prior existing grains and newly formed grains. The effect that temperature has on the evolution of this material can clearly be seen in the microstructures. Observing the samples annealed at 10s for the three temperatures, provides representation of how the microstructure is affected by change in temperature. The specimen annealed at 375°C still shows a large amount of dislocation as well as large amounts of nucleating grains. When the temperature is increased to 400°C, the dislocations are not as prominent. At this stage, some growth of nucleated grains can be observed, and a decrease in nucleation activity is witnessed. The sample annealed at 425°C shows an even more defined grain structure with less dislocation. At this point, only a few small regions of nucleation can be detected. The same trend can be said for the samples at the other annealing times. The samples annealed at higher temperatures are further along in the recrystallization and grain growth process. Such observations imply that as temperature is increased, the rate of recrystallization is increased as well. In addition to temperature affects, the effect annealing has on the samples corresponds with what has been witnessed in prior studies as well. A longer annealing time provides for a larger grain structure. Therefore, the rate of recrystallization and grain growth are increased by elevated temperatures.

The grain growth of the samples is observed to increase with rising annealing time and temperature as well. Although an average increase in grain size is witnessed for all of the samples, the grains seem to be divided into larger and smaller grains. The development of the grains observed in this process correlate well with what is described as abnormal grain growth. The grains do not all grow uniformly. Some of the grains appear to grow larger while certain smaller grains remain present.

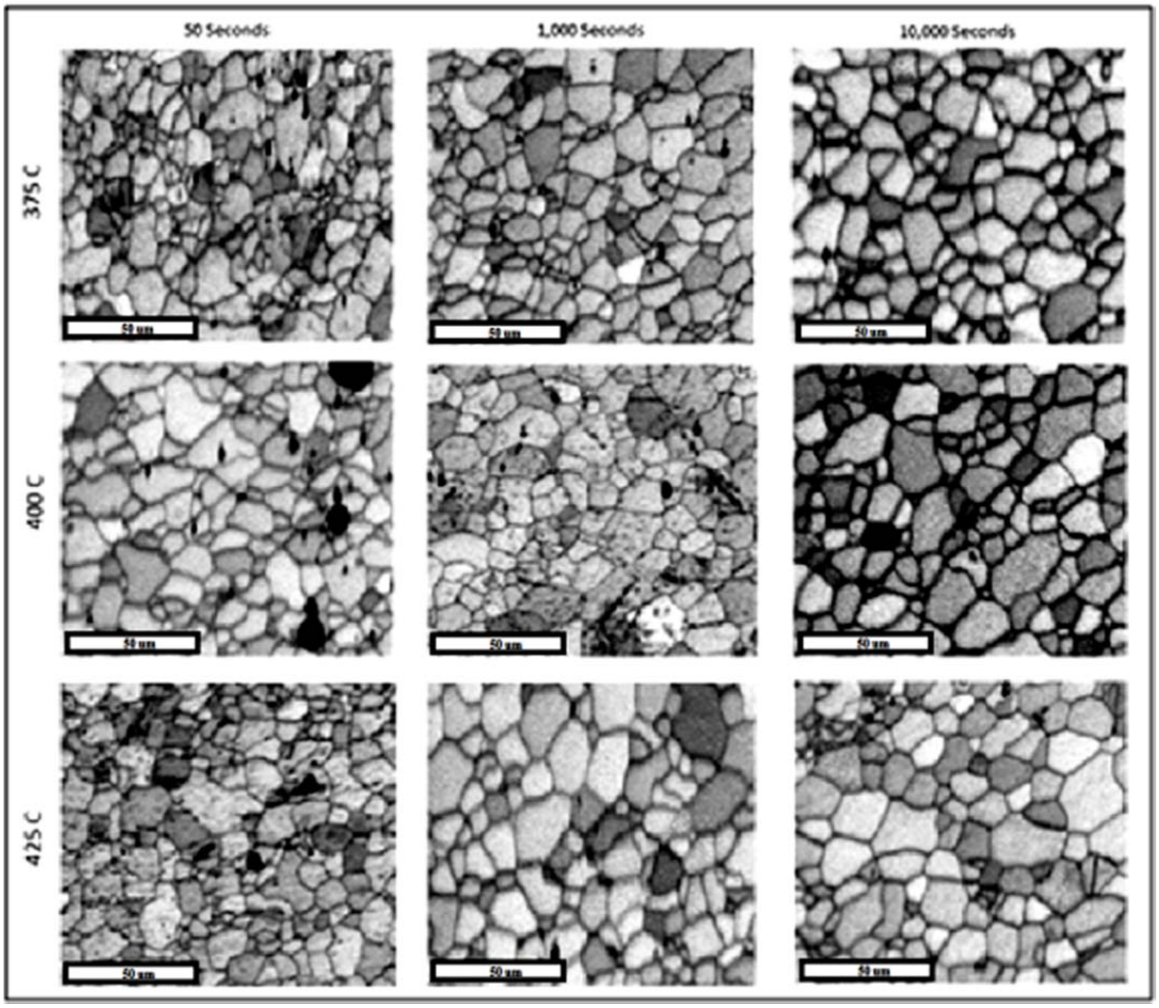

Figure 5.14 Images from EBSD scans representing the microstructural evolution of AZ31 TD samples for annealing times 50, 1,000, and 10,000s for the annealing temperatures 375°C, 400°C, and 425°C.

Optical images were taken of the RD samples as well. Although the as-deformed microstructures of the two sets of samples showed some variation, not much variation can be seen in the samples after the annealing process commences. In both the RD and TD samples, a series of optical images were collected during the annealing process. These are shown in Figures 5.15 and 5.16, respectively, to provide a comparison of the evolutionary processes.

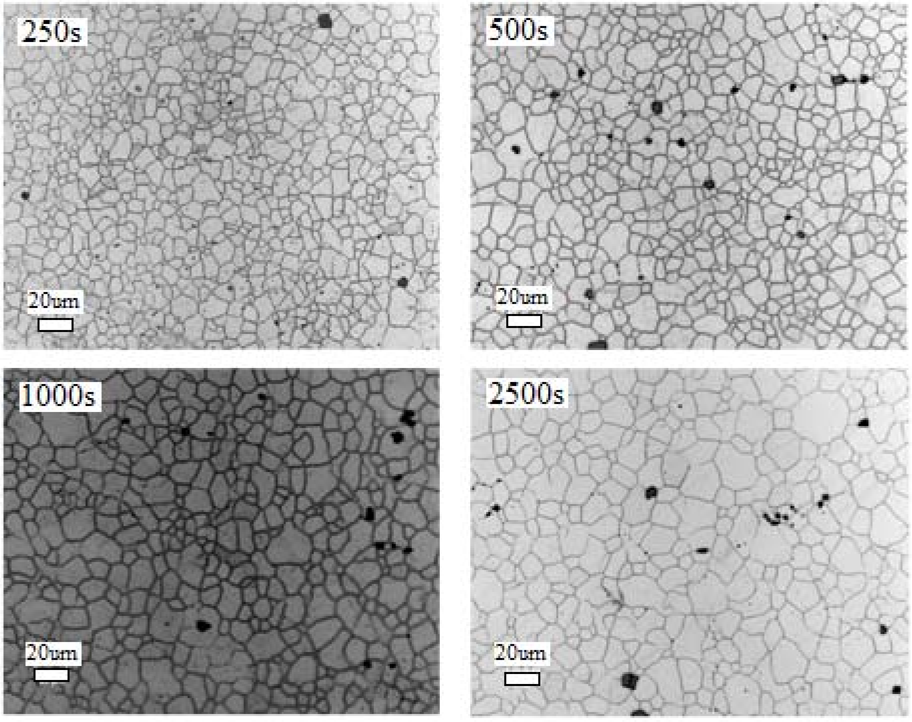

Figure 5.15 Optical images of RD samples annealed at 425°C for times 250, 500, 1000, and 2500 seconds.

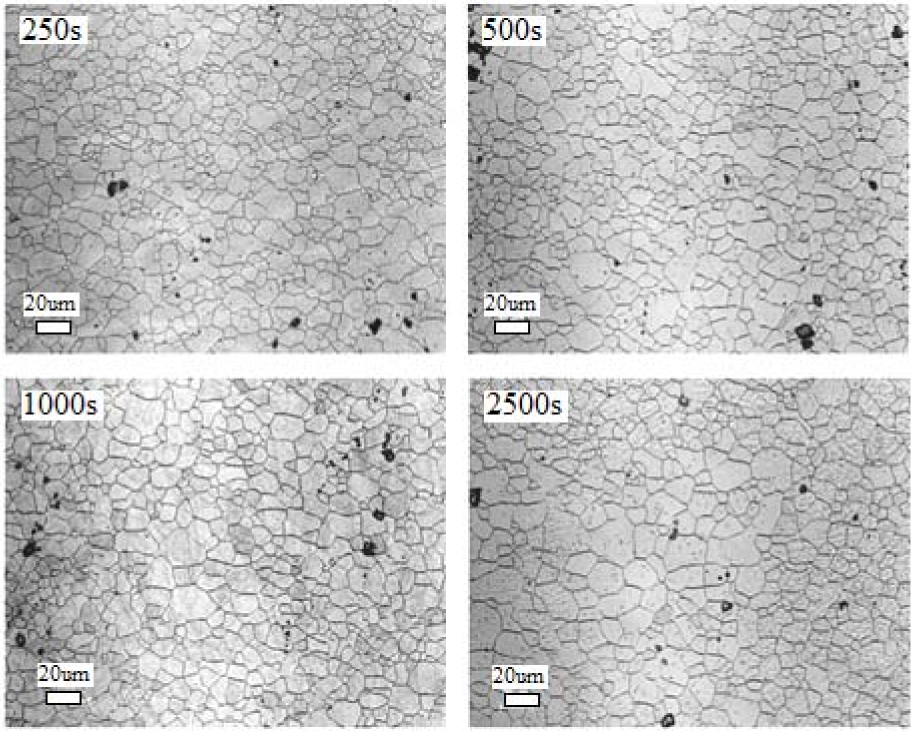

Figure 5.16 Optical images of TD samples annealed at 425°C for times 250s, 500s, 1000s, and 2500s.

5.5 Electron Backscatter Diffraction

One of the major advantages of electron backscatter diffraction (EBSD) is the ability to obtain multiple types of data with the completion of one scan. For this study, EBSD is utilized to obtain image maps of the grain structure, grain size data, and recrystallization data. Recrystallization has been studied using various measures of orientation including kernel average misorientation, a measure of local misorientation. Using a measure of the internal grain misorientation is a reasonable approach for examining recrystallization. Deformed grains have high densities of dislocations that are often organized into dislocation structures. On the other hand, recrystallized grains tend to have much lower dislocation densities. Dislocations generally result in local misorientations up to several degrees. The measured internal grain misorientation can directly be related to the dislocation density, and therefore, recrystallization.

5.5.1 Grain Size Analysis

Using the data collected from the EBSD scans, grain distribution charts were formed for each of the temperatures at several annealing times. Figure 5.17 displays the grain size distribution of the selected samples. What the charts display correlates well with what is observed in the optical images. The images obtained from both optical and EBSD displayed abnormal grain growth throughout the entire annealing process at all of the temperatures.

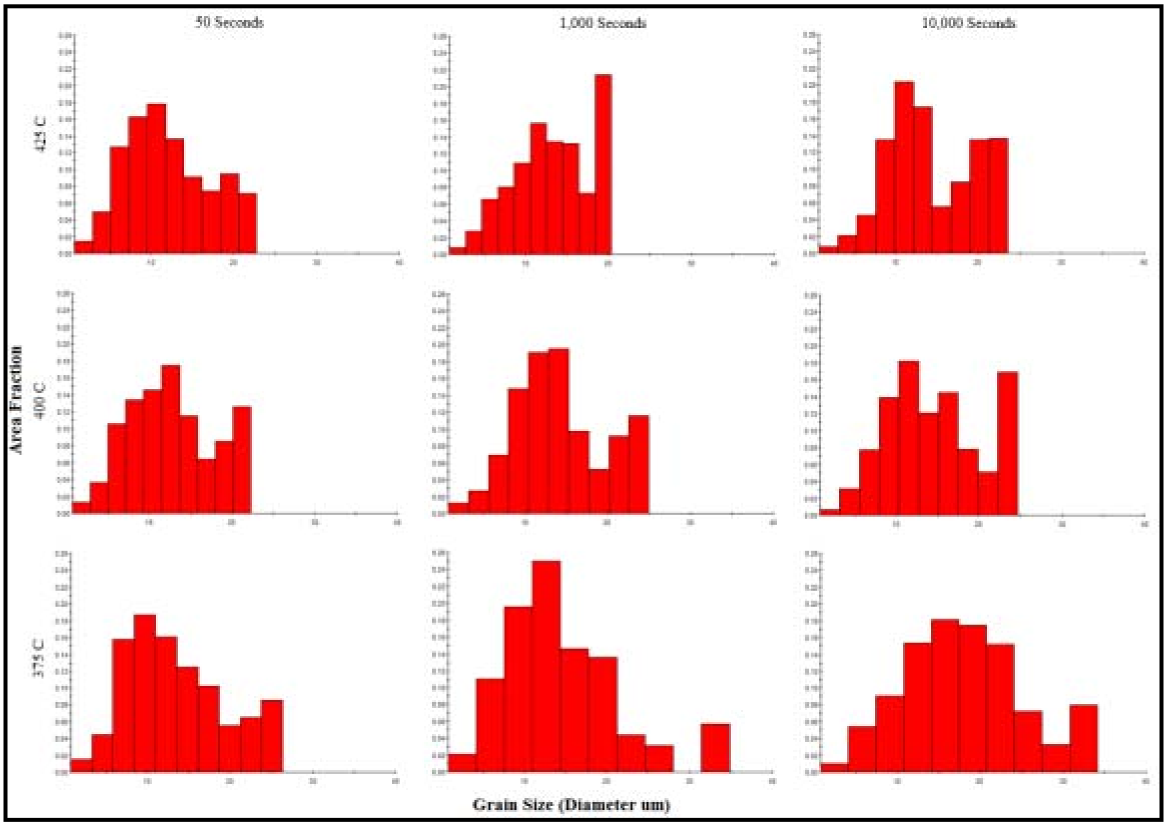

Figure 5.17 Grain size evolutions of the TD samples.

Each of the samples displays a bimodal distribution, signifying the presence of two sets of grain sizes among the microstructure. The variation in grain size among individual samples agrees with the abnormal grain growth theory, and what is observed in the optical images. The grain distribution charts provide data relating to grain size as well. Average grain size is calculated for each of the samples and the results are provided in Table 5.8

Table 5.8 Evolution of grain size (μm) of the TD samples.

	50s	**1000s**	**10000s**
375°C	12.026	13.26	14.36
400°C	12.719	14.295	15.342
425°C	13.31	14.736	18.182

The grain size data shows that the grain size increases with rising annealing time and temperature. In Figure 5.18, the grain size values are plotted against the annealing time to display the trend of grain growth for the three annealing temperatures. The grain growth patterns at both 375°C and 400°C show a similar trend. On the other hand, the first two points for the 425°C samples follows the same path as the lower temperatures. However, a large increase in grain size can be seen at 10,000s.

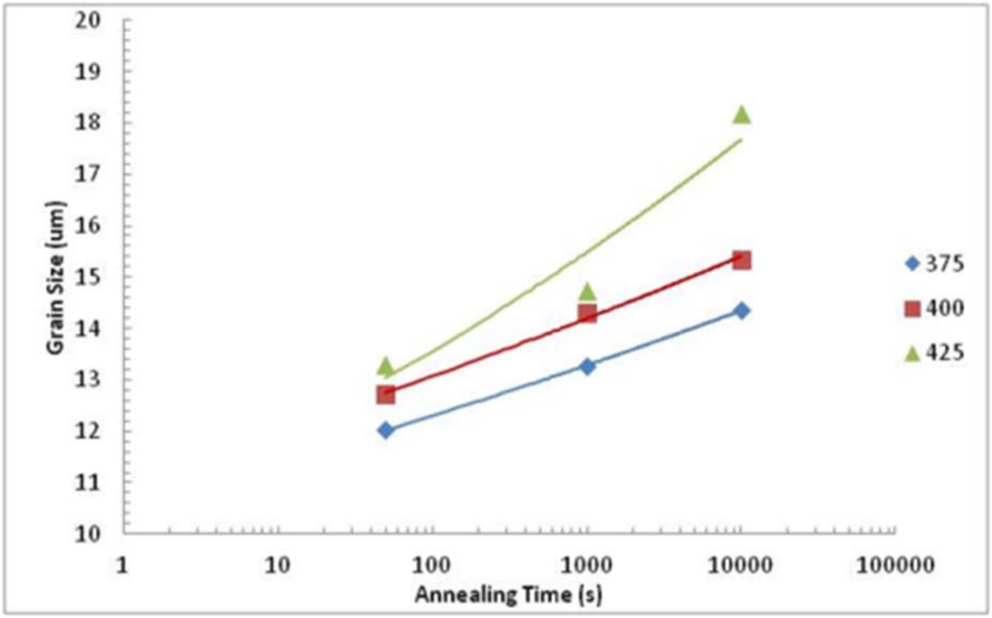

Figure 5.18 Grain size evolution in the TD samples at the three specified annealing temperatures.

Typically during the recrystallization process, an initial decrease in grain size would be observed, caused by the nucleation of new grains, and followed by an increase in size caused by growth of the new grains. However, only grain growth is observed in the samples annealed for 50s and longer. The absence of this initial decrease in grain size suggests that the majority of the recrystallization process has already occurred by this point, and that what is observed after the 50s point is mostly grain growth.

5.5.2 Grain Orientation (Texture)

The IPF map and texture plots for the as received material are displayed in Figure 5.19. The material has a strong 0001 orientation which can be attributed to the loading direction during the rolling process. Similarly the IPF maps for the compressed RD and TD samples are displayed in Figure 5.20. Both of the compressed samples display a very strong orientation in the 0001 direction as well.

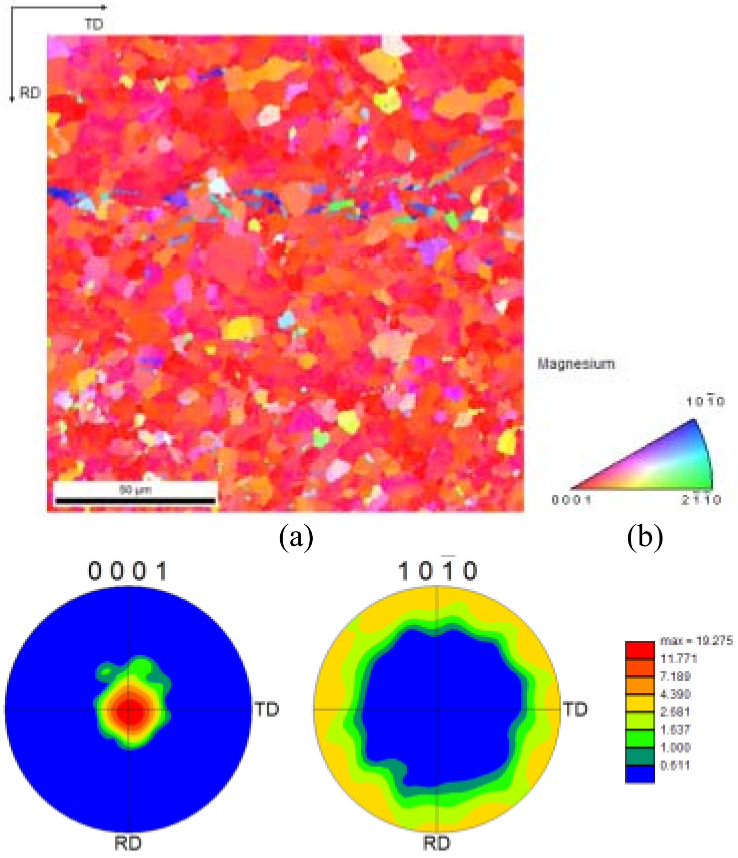

(a) (b)

(c) (d)

Figure 5.19 Microstructure and texture of the as-received material.

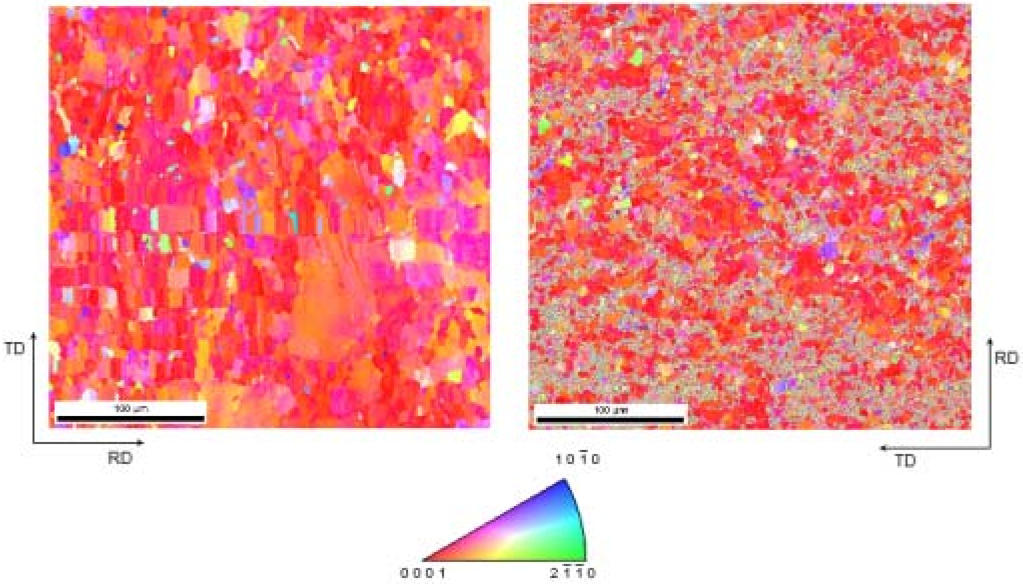

Figure 5.20 IPF Map of RD Sample (Left) and TD Sample (Right) after plane strain compression prior to annealing.

From observation of the IPF maps of the as received material and the compressed samples, the texture patterns for both cases are similar. However, a detailed comparison of the texture plots of the RD and TD samples, displayed in Figure 5.21, with that of the texture of the original material, reveals that the texture of the material is weekend through the deformation process. The as-received material displays a texture with max = 19.275. After channel die compression, the texture for the RD sample is decreased to a max = 12.235 while that of the TD sample to a max = 13.107.

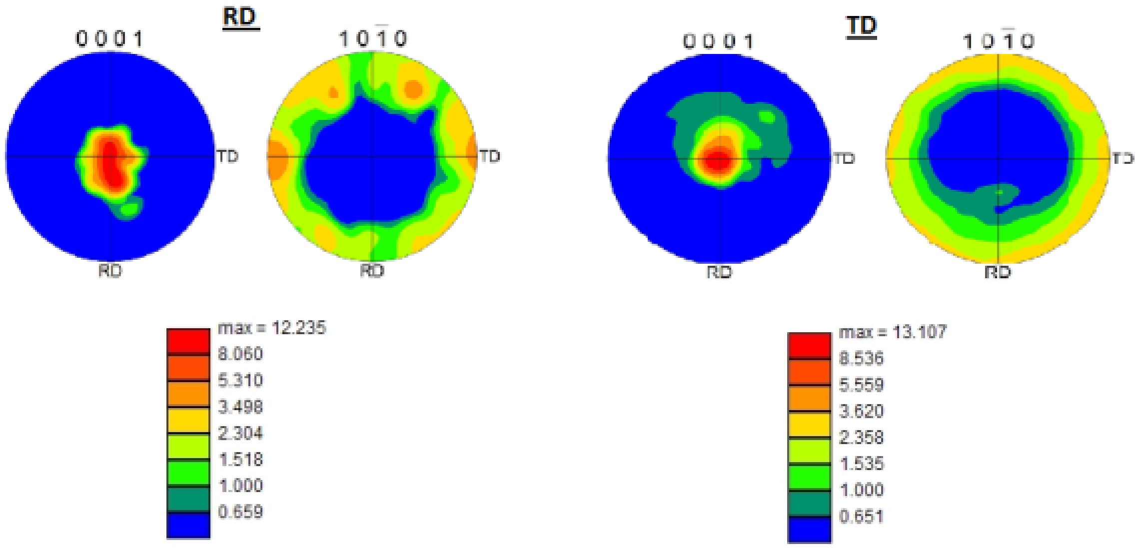

Figure 5.21 Texture of the compressed TD and RD samples before any annealing.

The texture evolution at each temperature was studied. Figure 5.22 represents the texture evolution for the chosen samples annealed at 400°C. All three temperatures displayed the same type of textural evolution. The annealing time does not seem to have an effect on the texture. For all samples, the texture did not vary much from that of its compressed state, regardless of annealing temperature. The idea that the texture does not evolve much throughout this process is to be somewhat expected. The material prior to compression exhibits a strong 0001 texture, and it is known that the grains of a recrystallizing structure typically tend to align themselves with respect to the loading direction. Therefore, since the material was loaded during compression along the same axis that the previous material's microstructure is aligned with, it is expected that there would not be a noticeable difference in texture between samples.

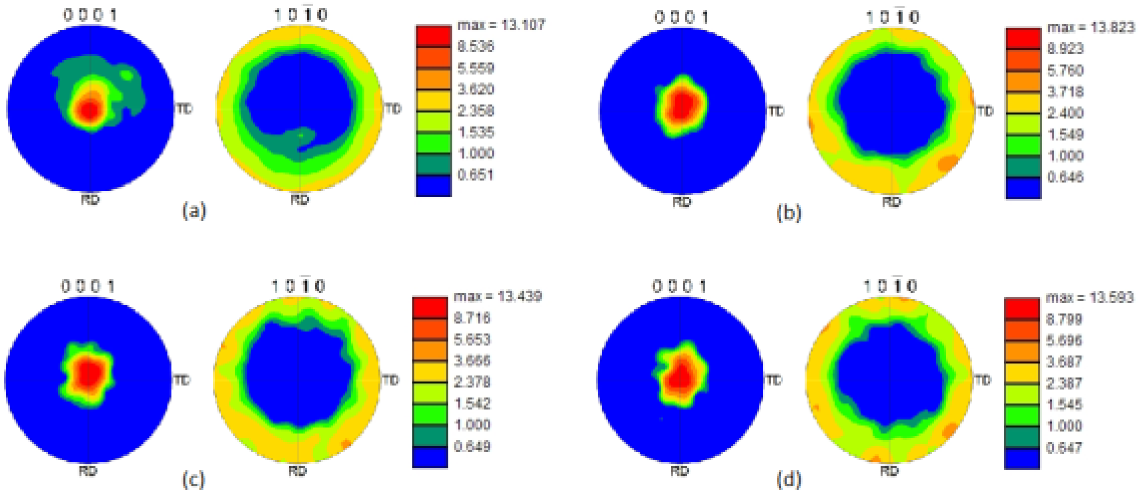

Figure 5.22 Texture evolution for samples annealed at 400°C. (a) Texture after compression before annealing. (b) After annealing for 250 seconds. (c) After annealing for 2,500 seconds. (d) After annealing for 10,000 seconds.

5.5.3 Fraction of Recrystallized Material From EBSD

If a material shows a continuous evolution of HAGBs from a low amount to a high amount, this value can be tracked to allow for the calculation of fraction Rex of the sample. A simple division between low-angle boundaries and high angle boundaries can be made by taking the separation angle to be 15°. The HAGB% can be obtained either from line scans or line analyses of area maps. Both methods give the same results, except the direct line scan method provides the same amount of data in a much shorter time. The fractional changes in the HAGB% during annealing can be used to measure the percentage of recrystallization (Rex%) by the following equation.

$$\text{Rex\%} = \frac{HAGB_T - HAGB_S}{HAGB_F - HAGB_S} \times 100 \tag{5.2}$$

where $HAGB_F$ is the fraction of HAGB in the fully recrystallized material, $HAGB_S$ is the fraction of HAGB for the material prior to recrystallization, and $HAGB_T$ is the fraction of HAGB after annealing for a period of time at a specified temperature. However, it has been observed that at high temperatures, the deformed microstructure can evolve homogeneously and gradually to an equiaxed grain structure by minor grain boundary movements and no observable nucleation and growth stages (Oscarsson et al., 1993; Humphreys et al., 1999: Humphreys and Hatherly 2003). In such situations, there is no significant change in the fraction of high angle boundaries on annealing (Jazaeri and Humphreys 2002). This process is known as continuous recrystallization, and typically occurs once the HAGB% in the deformed structure reaches 60-70%. Continuous recrystallization is usually promoted by a small initial grain size and larger strains.

The high angle grain boundaries for this process were observed for all three temperatures beginning with samples annealed at 50s. What is described as continuous recrystallization is observed for the material. No distinct change in the fraction of high angle boundaries is observed for all of the samples annealed for a time of 50 seconds or more and the percentage of HAGBs is larger than 70% for all samples. For cases such as this, other methods must be used in obtaining the Rex% for materials demonstrating continuous recrystallization. For microstructures determined using EBSD, it is convenient to select recrystallized material by assuming that it contains no detectable deformation within it. When concerned with EBSD, deformation can be detected in OIMs by significant misorientations between neighboring pixels. For measurements made from good patters, the misorientation sensitivity is slightly better than 0.3°. Therefore, for recrystallized material, it can be expected that the mean orientation between a pixel and all its close neighbors should be approximately this for recrystallized material. This average is better known as the kernel average. Very little of the stored energy of the material is within the regions with local misorientations less than 1°. Therefore, this fraction of the material can be defined as the recrystallized material.

The kernel average misorientation (KAM) was calculated for the as-received material and the as-deformed TD sample. A large difference can be seen between the two values. In Figure 5.24 the difference between the two samples is displayed by highlighted KAM maps. The as-received material displays a KAM<1 = 0.436. Upon compression, the KAM value drops significantly to 0.083. As the material is annealed and recrystallization proceeds, this value should increase. The KAM values for several samples at each temperature were calculated and are graphically represented in Figure 5.23. The KAM values reveal that at 50s, for all three temperatures, a large portion of the material has already been recrystallized. It is also observed that for the same annealing times, more of the material is recrystallized for samples at higher temperatures. The graphs indicate that the recrystallization process may be separated into two separate regimes. The first part of the recrystallization process appears to occur very rapidly before 50s of annealing. However, once the samples have been annealed for 50s, the fraction of recrystallization seems to have a gradual increase with continued annealing.

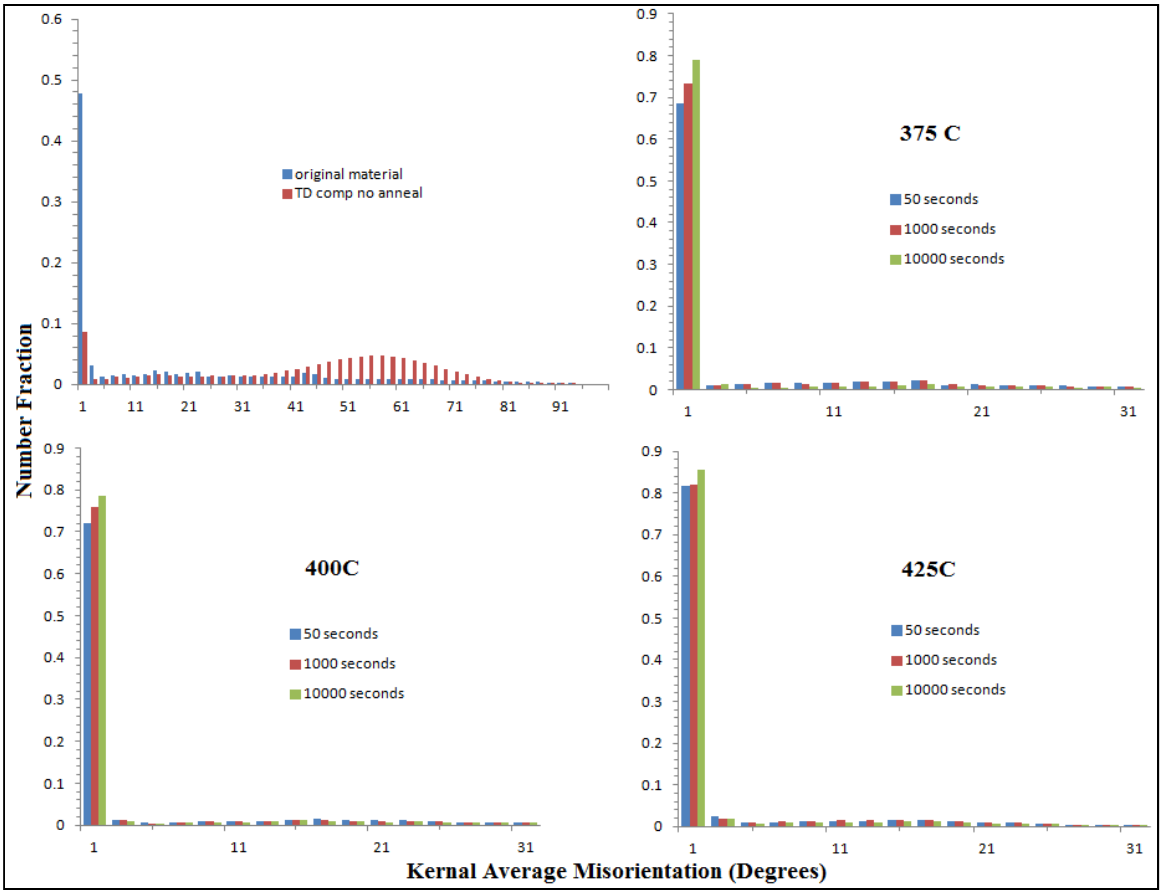

Figure 5.23 Comparison of the Kernal Average Misorientation values calculated for annealing times of 50s, 1000s, and 10000s for 375°C, 400°C, and 425°C.

The KAM evolution for samples at 400°C is represented in Figure 5.24. The blue colored section of the images represents material that has a KAM between 0 and 1. This portion of the material is considered to be recrystallized. We see that there is not much difference in the material that has been annealed for 50s and the material annealed for 10,000s. This trend is evident at all of the temperatures visually displayed by the large amount of blue and small amount of red color in the KAM map. Once the samples are annealed we see little change between the samples annealed for 50, 1000, and 10000 seconds. The values for these times are 0.755, 0.773, and 0.78 respectively.

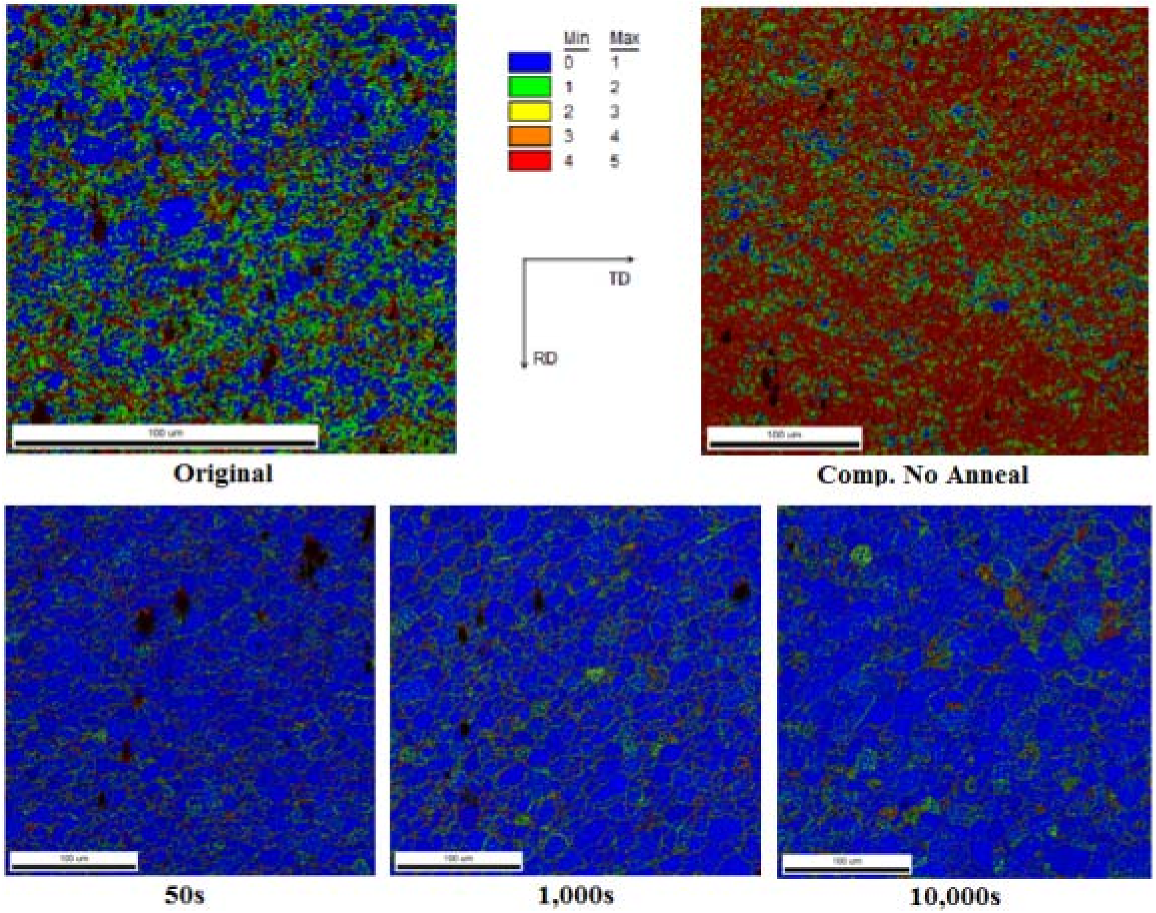

Original **Comp. No Anneal**

50s **1,000s** **10,000s**

Figure 5.24 Kernal average misorientation maps of the as received material, the material after compression at room temperature, and samples annealed at 400°C for 50s, 1000s, and 10000s.

Results similar to what is seen in this study were observed in pure magnesium by (Zou et al. 2009) . In his study, Zou traces the nucleation and grain growth during the static recrystallization of pure Mg. Based on the experimental data collected, they concluded that during the process there were two recrystallization kinetic regimes. At the early stages of annealing, the recrystallization occurred very rapidly which corresponded to a quick onset of recrystallization. However, after this initial rapid recrystallization regime, the recrystallized fraction slowly increased with annealing time. A plot displaying the data corresponding to the second recrystallization regime is provided in Figure 5.25.

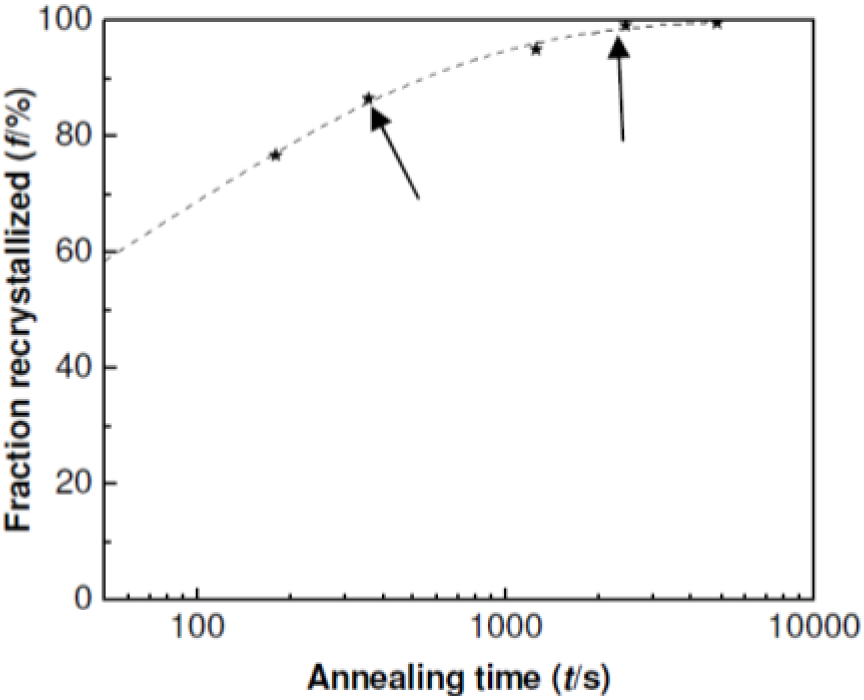

Figure 5.25 Trend in fraction of recrystallization of heat treated pure Mg. Two recrystallization regimes indicated by data. A rapid recrystallization at the early stages of annealing followed by a slow increase in recrystallized fraction with annealing time slowly approaching full recrystallization.

CHAPTER VI

MODELING STATIC RECRYSTALLIZATION OF AZ31

6.1 Introduction

The purpose of this section is to provide information about a common model used for recrystallization. The data used to fit this model is calculated using hardness and is a very rough estimate of the fraction of recrystallization of the actual material. However, from the experiments performed in this study, enough data was not collected from EBSD to span the entire process. Therefore, this model is used as a rough estimate to show how the model is created, and to also convey the potential need for a two step model that characterizes both the first and second regimes of recrystallization displayed by the static recrystallization process of this material.

6.2 JMAK Model

A very commonly used recrystallization model is the Johnson-Mehl_Avrami-Kolmogorov (JMAK) model. Many previous studies make use of this model to aid in the calculation of recrystallization kinetics, or as a method to verify their results (H. Lu et al. 2003)(Chao et al. 2011) (Su et al. 2008) (Winning & Schäfer 2006). The model assumes that nuclei are formed at a rate of $\dot{N}$ and grains grow into the deformed material at a linear rate of $\dot{G}$ and the fraction of recrystallized material (X_v) rises rapidly with time.

$$\dot{N} = C_1 \exp\left(-\frac{Q_N}{kT}\right)$$

$$\dot{G} = C_2 \exp\left(-\frac{Q_G}{kT}\right)$$

(6.1)

where C1 and C2 are constants, Q_N and Q_G are activation energies for nucleation and growth of nuclei respectively, k is the Boltzmann constant and T is the absolute temperature. The fraction of recrystallized material (X_v) is given by

$$X_v = 1 - \exp\left(-\frac{f\dot{N}\dot{G}^3 t^4}{4}\right)$$

(6.2)

where f is the shape factor (4π/3 for spheres) and t is time. Typically this equation is written as:

$$X_v = 1 - \exp(-Bt^n)$$

(6.3)

or

$$\ln\ln\left(\frac{1}{1 - X_v}\right) = \ln B + n \ln t$$

(6.4)

If the left side of the final equation is plotted against ln t, the Avrami exponent n can be obtained from the slope of the straight line. The value of n is equal to 4 if all the assumptions on which the model is built are satisfied. Using this method, and the relative hardness data as a rough estimate of the fraction of recrystallizatoin, the Avrami exponent is calculated using the JMAK model and presented in Figure 6.1.

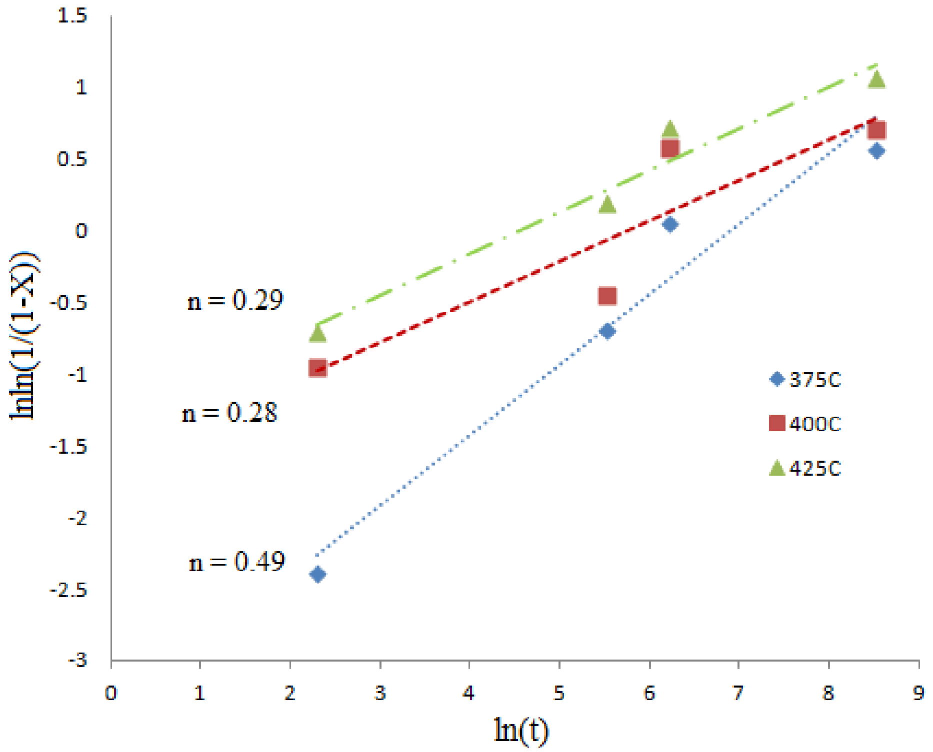

Figure 6.1 Recrystallization kinetics for static recrystallized AZ31 alloy by the JMAK plot using relative hardness values.

For similar studies, the Avrami exponent has been between 1 and 3. The low value of the exponent for this study can be caused by several things. First, relative hardness is used as the fraction of recrystallization as opposed to the fraction obtained from EBSD or optical microscopy (which has proven to be more accurate). Second, this model is used to fit data that experiences the commonly observed sinusoidal recrystallization. The results of this study did not display this type of trend in recrystallization however. Instead, it was observed that the material displayed the common sinusoidal trend at very early annealing times. But as the annealing times reached 50s, a more gradual rate of recrystallization was observed. It appears that the JMAK model will model the process, but only up to a certain annealing time. At some transition point the process must be modeled differently. From the data collected during this study, the transition point between the two regimes cannot be determined. Further work needs to be performed to investigate the phenomena and to better understand its effects.

CHAPTER VII

CONCLUSIONS AND FUTURE WORK

7.1 Introduction

It seems that for this particular study, the times chosen to capture the materials microstructure may have exceeded the recrystallization process. Using methods that have successfully given results in similar studies proved to yield data that did not seem to correlate with the recrystallization process. The optical images also defend this view. Grain growth respective to annealing time and temperature can clearly be seen. However, the nucleation and growth of new grains is unseen throughout the microstructural evolution. The microstructure images captured at 10s show a microstructure still in disarray from deformation, as well as dislocated grain boundaries and nucleating grains. However, when viewing the optical images beyond this annealing time, little to none of this activity is evident. From both the data and the optical images obtained, it is concluded that the bulk of the static recrystallization process for this type of compression must occur before the 50s time frame. This means that the process occurs at a very rapid rate and in order to be captured in the future, many samples must be tested in the early stages of the annealing process. Both the high strain at room temperature coupled with the high annealing temperatures for this alloy can be considered to aid in this rapid recovery process.

Based on the information gained through this study about the static recrystallization of the AZ31 alloy after channel die compression and annealing at the given temperatures, the following conclusions are made:

1. Based on Hardness and EBSD results, AZ31 after channel die compression at room temperature and heat treatment, showed trends that suggested a rapid recrystallization (before 50s) occurring at the early stages of annealing followed by a more gradual recrystallization occurring in the later stages of the annealing process.
2. Annealing Temperature had an effect on the change in hardness of the material. Samples that were annealed at higher temperatures displayed a faster rate of change in hardness than samples at lower temperatures.
3. Annealing Temperature also affected the microstructure of the material. Higher temperatures seemed to cause an earlier onset of recrystallization. Nucleation was observed in the 375°C sample at 10s. However samples annealed at the higher temperatures seemed to have already completed this process by this time. The grain size was also affected by temperature. At higher temperatures, the grain size typically increases at a faster rate and the final grain size is larger.
4. All three temperatures displayed what can be considered abnormal grain growth throughout the entire process. Even at the final annealing time, all temperatures showed a bimodal distribution of grain size, suggesting abnormal growth.
5. There was little difference seen between the RD and TD samples. There was some variation in the hardness values for the two sets, but the microstructures revealed very similar grain structures between the two sets of samples for all three temperatures.

6. Electron Backscattering Diffraction results displayed gradual change in samples annealed for 50s and beyond, as well as a large value of recrystallized grains for samples at these times. This suggests that large portions of the material are recrystallized at 50 seconds in the annealing process, and a second regime of recrystallization takes place in the later portion of annealing, that displays a slower recrystallization rate.
7. For a better understanding of the static recrystallization process of this material after channel die compression, a large set of samples should be compressed and studied at quick annealing times (before 100s) to capture the recrystallization process.

REFERENCES

Al-Samman, T. & Gottstein, G., 2008. Room temperature formability of a magnesium AZ31 alloy: Examining the role of texture on the deformation mechanisms. *Materials Science and Engineering: A*, 488(1-2), pp.406–414.

Banabic, D., 2000. *Formability of metallic materials: plastic anisotropy, formability testing, forming limits*, Springer Verlag.

Bay, B. et al., 1992. Overview no. 96 evolution of fcc deformation structures in polyslip. *Acta metallurgica et materialia*, 40(2), pp.205–219.

Beer, A. & Barnett, M., 2008a. Microstructure evolution in hot worked and annealed magnesium alloy AZ31. *Materials Science and Engineering: A*, 485(1-2), pp.318–324.

Beer, A. & Barnett, M., 2008b. Microstructure evolution in hot worked and annealed magnesium alloy AZ31. *Materials Science and Engineering: A*, 485(1-2), pp.318–324.

Brunet, M., Mguil, S. & Pol, P., 1998. Modelling of a roll-forming process with a combined 2D and 3D FEM code. *Journal of Materials Processing Technology*, 80, pp.213–219.

Cahn, R., 1950. A new theory of recrystallization nuclei. *Proceedings of the Physical Society. Section A*, 63, p.323.

Chao, H. et al., 2011. Static recrystallization kinetics of a heavily cold drawn AZ31 magnesium alloy under annealing treatment. *Materials Characterization*, 62(3), pp.312–320.

Choi, S.H., Kim, D., et al., 2011. 3-D simulation of spatial stress distribution in an AZ31 Mg alloy sheet under in-plane compression. *International Journal of Plasticity*.

Cottrell, A., 1953. Theory of dislocations. *Progress in metal physics*, 4, pp.205–264.

Dingley, D., 2004. Progressive steps in the development of electron backscatter diffraction and orientation imaging microscopy. *Journal of microscopy*, 213(3), pp.214–224.

Doherty, R., Hughes, D., et al., 1997. Current issues in recrystallization: a review. *Materials Science and Engineering A*, 238(2), pp.219–274.

Dziaszyk, S. et al., 2010. On the characterization of recrystallized fraction using electron backscatter diffraction: A direct comparison to local hardness in an IF steel using nanoindentation. *Materials Science and Engineering: A*, 527(29-30), pp.7854–7864.

Farag, M.M., 1990. *Selection of materials and manufacturing processes for engineering design*, Prentice Hall International (UK) Ltd.

Fatemi-Varzaneh, S., Zarei-Hanzaki, A. & Beladi, H., 2007. Dynamic recrystallization in AZ31 magnesium alloy. *Materials Science and Engineering: A*, 456(1-2), pp.52–57.

Gleiter, H. & Chalmers, B., 1972. High-Angle Grain-Boundaries. *Progress Mat. Sci., 1972, 16, 283 p.*

Grimmer, H., 1974. Disorientations and coincidence rotations for cubic lattices. *Acta Crystallographica Section A: Crystal Physics, Diffraction, Theoretical and General Crystallography*, 30(6), pp.685–688.

Guo, Q. et al., 2005. Behaviour of AZ31 magnesium alloy during compression at elevated temperatures. *Materials science and technology*, 21(11), pp.1349–1354.

Haasen, P., 1993. How are new orientations generated during primary recrystallization? *Metallurgical and Materials Transactions A*, 24(5), pp.1001–1015.

Haessner, F., 1978. Recrystallization of metallic materials. *Stuttgart, Dr. Riederer Verlag GmbH, 1978. 303 p.(For individual items see A 79-22802 to A 79-22807).*

Hamrock, B.J. et al., 1999. *Fundamentals of machine elements*, WCB/McGraw-Hill Singapore.

Hansen, N., Jensen, D., et al., 1995. Microstructural and crystallographic aspects of recrystallization.

Honeycombe, R.W.K. et al., 1968. *The plastic deformation of metals*, Edward Arnold London.

Humphreys, F., 1999. A new analysis of recovery, recrystallisation, and grain growth. *Materials science and technology*, 15(1), pp.37–44.

Humphreys, F.J. & Hatherly, M., 2004. *Recrystallization and related annealing phenomena*, Pergamon.

Jäger, A. et al., 2006. Influence of annealing on the microstructure of commercial Mg alloy AZ31 after mechanical forming. *Materials Science and Engineering: A*, 432(1-2), pp.20–25.

Jain, J., Poole, W. & Sinclair, C., 2006. A study on the static recrystallization of cold rolled magnesium alloy AZ80. *Mag. Tech., TMS, Warrendale PA*, pp.147–152.

Jazaeri, H. & Humphreys, F., 2004. Quantifying recrystallization by electron backscatter diffraction. *Journal of microscopy*, 213(3), pp.241–246.

Kobayashi, S., Oh, S.I. & Altan, T., 1989. *Metal forming and the finite-element method*, Oxford University Press, USA.

LEGERSKI, M. et al., MODEL OF STATIC RECRYSTALLIZATION OF MAGNESIUM ALLOY AZ31.

Lu, H., Sivaprasad, P. & Davies, C., 2003. Treatment of misorientation data to determine the fraction of recrystallized grains in a partially recrystallized metal. *Materials characterization*, 51(5), pp.293–300.

Martin, J.W., Doherty, R.D. & Cantor, B., 1997. *Stability of microstructure in metallic systems*, Cambridge Univ Pr.

Maurice, C. et al., 2005. Hot plane strain compression testing of aluminum alloys by channel-die compression. *Metallurgical and Materials Transactions A*, 36(4), pp.1039–1047.

Mccabe, R.J. & Teter, D.F., 2006. Analysis of recrystallized volume fractions in uranium using electron backscatter diffraction. *Journal of microscopy*, 223(1), pp.33–39.

Merkle, K. & Wolf, D., 1990. Structure and energy of grain boundaries in metals. *MRS Bulletin*, 15(9), pp.42–50.

Molodov, D. et al., 1995. Acceleration of grain boundary motion in Al by small additions of Ga. *Philosophical magazine letters*, 72(6), pp.361–368.

Nave, M.D. & Barnett, M.R., 2004. Microstructures and textures of pure magnesium deformed in plane-strain compression. *Scripta materialia*, 51(9), pp.881–885.

Prakash, A., Weygand, S. & Riedel, H., 2009. Modeling the evolution of texture and grain shape in Mg alloy AZ31 using the crystal plasticity finite element method. *Computational Materials Science*, 45(3), pp.744–750.

Raabe, D. et al., 2001. Micromechanical and macromechanical effects in grain scale polycrystal plasticity experimentation and simulation. *Acta materialia*, 49(17), pp.3433–3441.

Sediako, D. et al., 2007. Study of Texture Evolution During Channel-Die Compression of Mg-Al Alloys by In-Situ Neutron Diffraction. *Magnesium Technology 2007: TMS (The Minerals, Metals & Materials Society)*, pp.351–356.

Su, C.W., Lu, L. & Lai, M.O., 2008. Recrystallization and grain growth of deformed magnesium alloy. *Philosophical Magazine*, 88, pp.181-200.

Tucker, M.T. et al., 2009. Anisotropic effects on the strain rate dependence of a wrought magnesium alloy. *Scripta Materialia*, 60(3), pp.182–185.

Ulacia, I. et al., 2010. Mechanical behavior and microstructural evolution of a Mg AZ31 sheet at dynamic strain rates. *Acta Materialia*, 58(8), pp.2988–2998.

Volkert, C. & Lingk, C., 1998. Effect of compression on grain growth in Al films. *Applied physics letters*, 73, p.3677.

Walde, T. & Riedel, H., 2007. Modeling texture evolution during hot rolling of magnesium alloy AZ31. *Materials Science and Engineering: A*, 443(1-2), pp.277–284.

Wang, M., Zong, B. & Wang, G., 2008. A phase-field model to simulate recrystallization in an AZ31 Mg alloy in comparison of experimental data. *Journal of Materials Science and Technology*, 24(6).

Wilkinson, D. & Caceres, C., 1984. On the mechanism of strain-enhanced grain growth during superplastic deformation. *Acta Metallurgica*, 32(9), pp.1335–1345.

Winning, M. & Schäfer, C., 2006. Influencing recrystallization behaviour by mechanical loads. *Materials Science and Engineering: A*, 419(1), pp.18–24.

Zou, J., Jain, J. & Sinclair, C.W., 2009. Tracing Nucleation And Grain Growth During Static Recrystallization Of Pure Mg By EBSD. *Magnesium(Mg) Technology 2009*.

APPENDIX A

MAGNESIUM PREPARATION PROCESS

Step 1. Attach Rondo Disc and 1200 Silicon Carbide Paper to TegraPol

Set up polisher:

a. 300 RPM
b. Time – 30 s
c. Force – 10N
d. Water – On, pointed off to the side.

Dose with DP – Purple

Step 2. Attach 2400 Silicon Carbide Paper to TegraPol

Set up polisher:

a. 150 RPM
b. Time – 30 s
c. Force – 10N
d. Water – On, pointed off to the side.

Dose with DP – Purple

Step 3. Attach 4000 Silicon Carbide Paper to TegraPol

Set up polisher:

a. 150 RPM
b. Time – 2 minutes
c. Force – 10N
d. Water – On, pointed off to the side.

Dose with DP – Purple

Step 4. Attach MD MOL Cloth to TegraPol

Set up polisher:

a. 150 RPM
b. Time – 5 minutes
c. Force – 10N
d. Water – Off

Before Starting:

Squirt a Z pattern with DP Purple Lubricant on disc.
Put 3 drops of DP Suspension A (3u) on dis.

Start Polisher:

Drip 2 drops of suspension every 10s
Squirt Purple Lubricant (small amount) every 20s, just to keep moist

Step 5. Attach NAP Cloth to TegraPol

Set up polisher:

- a. 150 RPM
- b. Time – 2 minutes
- c. Force – 10N
- d. Water – Off

Before Starting:

Squirt a Z pattern with DP Purple Lubricant on disc.
Put 3 drops of DP Suspension A (1u) on dis.

Start Polisher:

Drip 2 drops of suspension every 10s
Squirt Purple Lubricant (small amount) every 20s, just to keep moist

Step 6. Attach MD Chem Cloth to LaboPol with platen guard

Set up polisher:

- a. 15 RPM
- b. Time – 45 minutes
- c. Force – 2.5N
- d. Water – Off

In a large jar, mix 100ml Ethylene Glycol (E178-4) and 2 popsicle sticks of Buehler MicroPolish II Alumina 0.05um. Use the automatic stirrer for 3 minutes to mix the solution, and apply heat for the first 2 minutes.